Journal of Computational Physics 227 (2008) 8448–8471

Contents lists available at ScienceDirect

Journal of Computational Physics

journal homepage: www.elsevier.com/locate/jcp

A stabilized stochastic finite element second-order projection method for modeling natural convection in random porous media

Xiang Ma, Nicholas Zabaras *

Materials Process Design and Control Laboratory, Sibley School of Mechanical and Aerospace Engineering, 101 Frank H.T. Rhodes Hall, Cornell University, Ithaca, NY 14853-3801, USA

ARTICLE INFO

Article history:
Received 15 April 2007
Received in revised form 6 March 2008
Accepted 5 June 2008
Available online 21 June 2008

Keywords:
Natural convection
Random porous media
Stochastic finite element method
Stochastic projection method
Sparse grid collocation
Stabilized finite element method

ABSTRACT

We consider natural convection in flow saturated porous media with random porosity. The porosity is treated as a random field and a stochastic finite element method is developed. The stochastic projection method is considered for the solution of the high-dimensional stochastic Navier–Stokes equations since it leads to the uncoupling of the velocity and pressure degrees of freedom. Because of the porosity dependence of the pressure gradient term in the governing flow equations, one cannot use the first-order projection method. A stabilized stochastic finite element second-order projection method is presented based on a pressure gradient projection. A two-dimensional stochastic problem with moderate and large variation in the random porosity field is examined and the results are compared with Monte-Carlo and sparse grid (Smolyak) collocation approaches. Excellent agreement between these results indicates the effectiveness and accuracy of the proposed methodology.

© 2008 Elsevier Inc. All rights reserved.

1. Introduction

Fluid flow through porous media is an ubiquitous process occurring in various applications such as fluidized beds, solidification of alloys, geothermal energy systems and oil recovery. The analysis of flow through a medium with deterministic porosity has been well studied [1]. However, in practice, only limited statistical information is available regarding the structure and material properties of the medium. These statistics are easily extracted and reconstructed from experimental data. The porosity can thus be conveniently described by random fields. This enables us to develop a methodology that treats the porosity as input uncertainty and analyzes the propagation of this uncertainty through the governing equations of thermal and flow transport.

In this context, a number of methods have been proposed [2–7] that however are limited to small fluctuations and do not provide higher-order statistics of the solution. A more effective technique is the spectral stochastic finite element method (SSFEM) [8]. In this method, the random field is discretized directly, i.e., uncertainty is treated as an additional dimension along with space and time and a field variable is expanded along the uncertain dimension using suitable expansions. The most widely used expansions are the Karhunen–Loève expansion (KLE) and the polynomial chaos expansion (PCE). In PCE, Gaussian random variables are used with Hermite polynomials to represent a second-order stochastic process. This was extended to the generalized polynomial chaos expansion (GPCE), which uses the Wiener–Askey orthogonal polynomials [9]. The SSFEM has been widely used in fluid flow simulations [10–12].

* Corresponding author. Tel.: +1 607 255 9104; fax: +1 607 255 1222.
E-mail address: zabaras@cornell.edu (N. Zabaras).
URL: http://mpdc.mae.cornell.edu/ (N. Zabaras).

0021-9991/$ - see front matter © 2008 Elsevier Inc. All rights reserved.
doi:10.1016/j.jcp.2008.06.008

During the past few years, a number of works have been reported using the GPCE method driven by a K–L expansion to discretize the random porosity [13–18]. Others used the so called KL-based moment-equation approach [19–21]. Most of these works focused on either thermal diffusion or flow motion. There is no detailed analysis as of today that accounts for both thermal and momentum transport (e.g., natural convection) in such random porous media. In order to reduce the problem complexity and decouple the calculation of velocity and pressure, a stochastic projection method was developed based on the first-order projection method and was applied successfully to natural convection in a closed cavity [22–25]. However, in porous media flow, due to the porosity dependence of the pressure gradient term in the momentum equation, we cannot impose the divergence-free constraint as is the case in the first-order projection method [26]. Thus, in order to model uncertainty propagation in natural convection in random heterogeneous porous media we need to extend the stochastic projection formulation to the second-order projection approach. This is one of the primary contributions of this paper.

The projection method for the incompressible Navier–Stokes equations, also known as the fractional step method or operator splitting method, has attracted widespread popularity [27]. The reason for this lies on the uncoupling of the velocity and pressure computation. It was first introduced as the first-order projection method (also called non-incremental pressure-correction method) [28]. Later, it was extended to the second-order scheme (also called incremental pressure-correction scheme) in which part of the pressure gradient is kept in the momentum equation [29,30]. These techniques either employ spectral or finite differences techniques and it is not straightforward to extend them to a finite element interpolation. As it is known, the approximation spaces for velocity and pressure must a priori satisfy the *inf–sup* condition, otherwise, there will be a severe node-to-node spatial oscillation in the pressure field [31]. The first-order projection method has some pressure stability control which depends on the time step size. However, there is a severe node-to-node spatial pressure oscillation for a second-order scheme if we do not satisfy the *inf–sup* condition (e.g., by using a mixed finite element formulation for velocity and pressure).

In order to utilize the advantage of the incremental projection method which retains the optimal space approximation property of the finite element and allows equal-order finite element interpolation, a pressure stabilized finite element second-order projection formulation for the incompressible Navier–Stokes equations has been developed [32–35]. This method mimics the stabilizing effect of the first-order projection method. It consists of introducing the projection of pressure gradient and adding the difference between the Laplacian of the pressure and the divergence of this new field to the incompressibility equation. Following this idea, we developed a framework of pressure stabilized stochastic second-order projection method. This paper is organized as follows: In Section 2, a brief review of the deterministic problem definition and second-order projection method is given. A framework for representing stochastic processes is presented in Section 3. Various issues related to modeling the uncertainties in heterogeneous porous media are detailed in Section 4. Example problems are presented in Section 5. Results are compared with those obtained through Monte-Carlo and the sparse grid collocation approach discussed in [36]. Finally, concluding remarks and future suggestions are given in Section 6.

2. Deterministic problem formulation

2.1. Problem statement

A generalized non-Darcian porous medium model for natural convective flow has been developed in [1] that includes linear and non-linear matrix drag components as well as the inertial and viscous forces within the fluid. In [37], a similar model was utilized using a volume-averaged method. Here, we just present the governing equations. For detailed derivation, the interested reader may refer to the above papers.

Consider a d-dimensional bounded domain $D \subset \mathbb{R}^d$ with a boundary $\partial D_{\mathrm{d}} \bigcup \partial D_{\mathrm{n}}$. Dirichlet boundary conditions are applied on ∂D_{d}, while Neumann boundary conditions are applied on ∂D_{n}. The problem consists of finding the velocity $\boldsymbol{v}$, pressure p and temperature θ such that the following non-dimensional governing equations are satisfied:

$$\frac{\partial \boldsymbol{v}}{\partial t} + \frac{\boldsymbol{v}}{\epsilon} \cdot \nabla \boldsymbol{v} = -\frac{Pr}{Da} \frac{(1-\epsilon)^2}{\epsilon^2} \boldsymbol{v} - \frac{1.75\|\boldsymbol{v}\|(1-\epsilon)}{(150Da)^{1/2}\epsilon^2} \boldsymbol{v} + Pr\nabla^2 \boldsymbol{v} - \epsilon \nabla p - \epsilon PrRa\theta \mathbf{e}_{\mathrm{g}}, \tag{1}$$

$$\nabla \cdot \boldsymbol{v} = 0, \tag{2}$$

$$\frac{\partial \theta}{\partial t} + \boldsymbol{v} \cdot \nabla \theta = \nabla^2 \theta, \tag{3}$$

where ϵ is the porosity of the medium and $\mathbf{e}_{\mathrm{g}}$ is the unit vector in the direction of gravity. The other important non-dimensional parameters are the Prandtl number Pr, Darcy number Da and the thermal Rayleigh number Ra. Also, we assume the Boussinesq approximation is satisfied and that appropriate boundary conditions are imposed.

2.2. Pressure stabilized formulation

We will discuss the pressure stabilized second-order projection method formulation based on the pressure projection. For detailed discussion and derivation, the interesting reader may refer to [33,35]. The method consists in adding to the

incompressibility equation the divergence of the difference between the pressure gradient and its projection onto the velocity space, both multiplied by algorithmic parameters defined element-wise. We take these parameters as in [34]

$$\tau_e := \left[\left(c_1 \frac{v}{h_e^2} \right)^2 + \left(c_2 \frac{\|\boldsymbol{v}_h\|}{h_e} \right)^2 \right]^{-1/2}, \tag{4}$$

where v is the viscosity, h_e is the local size of the element $\boldsymbol{e}$, $\|\boldsymbol{v}_h\|$ is the local velocity and c_1 and c_2 are algorithmic constants, which we take as $c_1 = 4$ and $c_2 = 2$ for linear elements and $c_1 = 16$ and $c_2 = 4$ for quadratic elements.

Having introduced these parameters, the continuity equation is modified as follows:

$$-\tau \nabla^2 p + \tau \nabla \cdot \boldsymbol{\pi} + \nabla \cdot \boldsymbol{v} = 0, \tag{5}$$

$$-\nabla p + \boldsymbol{\pi} = 0, \tag{6}$$

where τ is the stabilized parameter as discussed before and the new auxiliary variable $\boldsymbol{\pi}$ is the projection of the pressure gradient ∇p onto the velocity space. Eq. (5) is the modified continuity equation.

2.3. Stabilized second-order projection method

Let us denote with superscript n the value of each variable at the end of the nth time step and with Δt the time step. The second-order projection method corresponding to Eqs. (1), (3), (5), (6) consists of the following three major steps [35]:

Step 1. Solve for the intermediate velocity $\boldsymbol{v}^{n+1/2}$ in the momentum equation:

$$\begin{aligned} \frac{1}{\Delta t}(\boldsymbol{v}^{n+1/2} - \boldsymbol{v}^n) + 2\frac{\boldsymbol{v}^n}{\epsilon} \cdot \nabla \boldsymbol{v}^n - \frac{\boldsymbol{v}^{n-1}}{\epsilon} \cdot \nabla \boldsymbol{v}^{n-1} = & -\frac{Pr}{Da} \frac{(1-\epsilon)^2}{\epsilon^2}(2\boldsymbol{v}^n - \boldsymbol{v}^{n-1}) - \frac{1.75\|\boldsymbol{v}^n\|(1-\epsilon)}{(150Da)^{1/2}\epsilon^2}(2\boldsymbol{v}^n - \boldsymbol{v}^{n-1}) \\ & + Pr\nabla^2 \boldsymbol{v}^{n+1/2} - \epsilon \nabla p^n - \epsilon PrRa\theta^n \mathbf{e}_g. \end{aligned} \tag{7}$$

In the first-order projection method, the pressure gradient term $-\epsilon \nabla p^n$ is neglected in this equation. It is important to understand that the intermediate velocity $\boldsymbol{v}^{n+1/2}$ does not satisfy the continuity (divergence-free) constraint. Thus, we employ the following projection step.

Step 2. Projection step

$$\frac{(\boldsymbol{v}^{n+1} - \boldsymbol{v}^{n+1/2})}{\Delta t} + \nabla(p^{n+1} - p^n) = 0, \tag{8}$$

$$-\tau \nabla^2 p^{n+1} + \tau \nabla \cdot \boldsymbol{\pi}^n + \nabla \cdot \boldsymbol{v}^{n+1} = 0. \tag{9}$$

A common approach to avoid using a mixed finite element interpolation is to use the pressure Poisson equation. In particular, we take the divergence of Eq. (8) and make use of Eq. (9) to yield

$$(\Delta t + \tau)\nabla^2 p^{n+1} = \Delta t \nabla^2 p^n + \nabla \cdot \boldsymbol{v}^{n+1/2} + \tau \nabla \cdot \boldsymbol{\pi}^n. \tag{10}$$

In this equation, $p^n, \boldsymbol{v}^{n+1/2}$ and $\boldsymbol{\pi}^n$ are known quantities from the previous step. Thus, we can solve for p^{n+1}. Note that the boundary condition for this equation are homogeneous Neumann boundary conditions [28]. In addition, the pressure at a given point (here at (0, 0)) is fixed at zero value.

Step 3. Finally, we update $\boldsymbol{\pi}^{n+1}$, velocity $\boldsymbol{v}^{n+1}$ and temperature θ^{n+1} according to

$$\boldsymbol{\pi}^{n+1} = \nabla p^{n+1}, \tag{11}$$

$$\boldsymbol{v}^{n+1} = \boldsymbol{v}^{n+1/2} - \Delta t(\nabla p^{n+1} - \nabla p^n), \tag{12}$$

$$\frac{\theta^{n+1} - \theta^n}{\Delta t} + 2\boldsymbol{v}^n \cdot \nabla \theta^n - \boldsymbol{v}^{n-1} \cdot \nabla \theta^{n-1} = \nabla^2 \theta^{n+1}. \tag{13}$$

Note that Eqs. (7) and (10)–(13) provide a complete solution to the problem and are fully-decoupled. Thus, we can first solve for the intermediate velocity $\boldsymbol{v}^{n+1/2}$ from Eq. (7) and then solve the pressure from Eq. (10). Finally, we update $\boldsymbol{\pi}^{n+1}$, velocity $\boldsymbol{v}^{n+1}$ and temperature θ^{n+1} according to Eqs. (11)–(13). Each of them is a rather simple equation that can be easily solved using the finite element method. This enables us to introduce next the GPCE formulation of this problem.

3. Representation of stochastic processes

Consider a complete probability space $(\Omega, \mathcal{F}, \mathcal{P})$ with sample space Ω which corresponds to the outcomes of some experiments, the σ-algebra $\mathcal{F}$ of subsets of Ω (these subsets are called events) and the probability measure $\mathcal{P}$ on $\mathcal{F}$. The uncertainty

is modeled as a second-order stochastic process, which is a process that has finite variance. In subsequent sections, any quantity with an ω-dependence represents a stochastic quantity and $\omega \in \Omega$. Theoretically, the stochastic process can be represented as a random variable at each spatial and temporal location. Therefore, we require an infinity number of random variables to completely characterize a stochastic process. This poses a numerical challenge in modeling uncertainty in physical quantities that have spatio-temporal variations, hence necessitating the need for a reduced-order representation. In this section, we will consider two most popular ways of approximating a second-order stochastic process using a truncated spectral expansion comprising of a few random variables: (a) approximation by the Karhunen–Loève expansion (K–L) [8] and (b) approximation by the generalized polynomial chaos expansion (GPCE) [9,10].

3.1. Karhunen–Loève expansion

The most common approach for representing input uncertainty is the K–L expansion, which is optimal in the sense that the mean-square error of the finite representation of the process $\epsilon(\mathbf{x},\omega)$ (in our problem random porosity) is minimized. Let us denote the process by $\epsilon(\mathbf{x},\omega)$ and its correlation function by $R_{hh}(\mathbf{x},\mathbf{y})$, where $\mathbf{x}$ and $\mathbf{y}$ are spatial coordinates. By definition, the correlation function is real, symmetric and positive definite. All its eigenfunctions are mutually orthonormal and form a complete set spanning the function space to which $\epsilon(\mathbf{x},\omega)$ belongs. The K–L expansion then takes the following form:

$$\epsilon(\mathbf{x},\omega) = \bar{\epsilon}(\mathbf{x}) + \sum_{i=1}^{\infty} \sqrt{\lambda_i} f_i(\mathbf{x}) \xi_i(\omega), \tag{14}$$

where $\bar{\epsilon}(\mathbf{x})$ denotes the mean of the random process, and $\boldsymbol{\xi} = \{\xi_i(\omega)\}_{i=1}^{\infty}$ forms a set of uncorrelated random variables. If the process is a Gaussian process, then they are standard identically independent $N(0,1)$ Gaussian random variables. Also, $f_i(\mathbf{x})$ and λ_i are the eigenfunctions and eigenvalues of the correlation function, respectively. They are the solutions from the following eigenvalue problem:

$$\int R_{hh}(\mathbf{x},\mathbf{y}) f_i(\mathbf{y})\, d\mathbf{y} = \lambda_i f_i(\mathbf{x}). \tag{15}$$

We can solve this equation numerically [8,38]. The K–L expansion provides an effective way to represent the input uncertainties which have a spatial variation such as material properties when their correlation structure is known. Also note that we always truncate the expansion into finite number of terms. The number of expansion terms represents the stochastic dimensions used in the problem.

The final form of the truncated K–L expansion is as follows:

$$\epsilon(\mathbf{x},\omega) = \bar{\epsilon}(\mathbf{x}) + \sum_{i=1}^{M} \sqrt{\lambda_i} f_i(\mathbf{x}) \xi_i(\omega), \tag{16}$$

where M is the truncated number of terms, which denotes the stochastic dimension in the problem.

We use the scalable library SLEPc for eigenvalue problem computations [39]. SLEPc is based on the PETSc [40] data structure and it employs the MPI standard for message-passing communication for parallel high performance computation.

3.2. Generalized polynomial chaos expansion

The polynomial chaos (PC) expansion technique for representation of L_2-random processes was originally described in [41]. This constituted representing the random process as an expansion in terms of Hermite polynomials in the random space (a trial basis for $L_2(\Omega)$). An extension to the original polynomial chaos expansion technique was introduced in [9], where hypergeometric orthogonal polynomials from the Askey series in the random space were used as a trial basis for $L_2(\Omega)$.

We represent the general second-order random process $X(\omega)$, which is a process with finite variance, as

$$X(\omega) = a_0 \Gamma_0 + \sum_{i_1=1}^{\infty} a_{i_1} \Gamma_1(\xi_{i_1}(\omega)) + \cdots + \sum_{i_1=1}^{\infty} \cdots \sum_{i_n=1}^{i_{n-1}} a_{i_1 i_2 \ldots i_n} \Gamma_n(\xi_{i_1}(\omega), \ldots, \xi_{i_n}(\omega)) + \cdots, \tag{17}$$

where $\Gamma_n(\xi_{i_1}(\omega), \ldots, \xi_{i_n}(\omega))$ denote the Wiener–Askey polynomial chaos of order n in terms of the uncorrelated random vector $\boldsymbol{\xi} := (\xi_{i_1}(\omega), \ldots, \xi_{i_n}(\omega))$. In the original polynomial chaos, $\{\Gamma_n\}$ are multi-dimensional Hermite polynomials and $\boldsymbol{\xi}$ are orthonormal standard Gaussian random variables. In the GPCE, however, $\{\Gamma_n\}$ and $\boldsymbol{\xi}$ are inter-related through the joint PDF of $\boldsymbol{\xi}$. For example, gamma distribution corresponds to Laguerre polynomials and uniform distribution corresponds to Legendre polynomials [9]. Since in our problem the porosity is modeled as Gaussian random filed, Hermite polynomials are used in the PC expansion.

For notational convenience, Eq. (17) can be rewritten as

$$X(\omega) = \sum_{j=0}^{\infty} \hat{a}_j \Psi_j(\boldsymbol{\xi}), \tag{18}$$

where, the equality is interpreted in the $L_2(\Omega)$ sense and there is a one-to-one correspondence between $\Gamma_n(\xi_{i_1}(\omega),\ldots,\xi_{i_n}(\omega))$ and $\Psi_j(\xi)$. Since each type of polynomial in the Askey-series forms a complete basis for $L_2(\Omega)$, we can expect the GPCE to converge to any L_2 random process in the mean-square sense. The orthogonality relation of the Wiener–Askey polynomial chaos takes the form

$$\langle \Psi_i \Psi_j \rangle = \langle \Psi_i^2 \rangle \delta_{ij}, \tag{19}$$

where δ_{ij} is the Kronecker delta and $\langle \cdot,\cdot \rangle$ denotes the ensemble average, which is the inner product in the Hilbert space of the variables ξ,

$$\langle f(\xi) g(\xi) \rangle = \int f(\xi) g(\xi) W(\xi)\, \mathrm{d}\xi. \tag{20}$$

Here, $W(\xi)$ is the weighting function corresponding to the Wiener–Askey polynomial chaos basis Ψ_j [9]. Note that, some types of orthogonal polynomials from the Askey scheme have weighting functions the same as the probability function of certain types of random distributions. For example, the weighting function of the p-dimensional Hermite polynomial is just the probability density function of multivariate standard normal distribution, i.e.,

$$W(\xi) = \frac{1}{\sqrt{(2\pi)^p}} \mathrm{e}^{-\frac{1}{2}\xi^{\mathrm{T}}\xi}. \tag{21}$$

In practice, we then choose the type of independent variables ξ in the polynomials $\{\Psi_j(\xi)\}$ according to the type of random distribution and truncate the expansion at finite term P, i.e.,

$$X(\omega) = \sum_{j=0}^{P} \hat{a}_j \Psi_j(\xi). \tag{22}$$

The total number of expansion terms is $(P+1)$ and is determined by the dimension (M) of random vector ξ and the highest order (n) of the polynomials $\{\Psi_j\}$:

$$P + 1 = \frac{(n+M)!}{n!M!}. \tag{23}$$

We choose a suitable order of the GPCE to capture strong non-linear dependence of the solution process on the input uncertainty (uncertainty quantification or uncertainty propagation process).

Remark 1. The truncated GPCE expansion is characterized by the stochastic dimension and the order of the expansion. The stochastic dimension is determined by the number of terms M in the truncated K–L expansion of the input random processes. Since the accuracy of the truncated GPCE depends on the order of the expansion, we require techniques to determine the optimal truncation order. We use the weak-Cauchy convergence criterion for this purpose [13]. Let the guess for optimal order be q. Then we construct an order m GPCE, where $m = q+1, q+2$. In the criterion, we require that the L_2 norm of the difference in the two approximations be negligible. Note the convergence should hold point-wise and these checks are made a priori in order to determine the optimal order of the GPCE.

4. Stochastic finite element method formulation

In this section, we will present the complete stochastic finite element formulation for this problem.

4.1. Non-polynomial function evaluations of stochastic spectral expansion

First, let us determine the spectral expansion of the product of the form $c = ab = \sum_{i=0}^{P} c_i \Psi_i(\xi)$, where a and b are given by

$$a(\xi) = \sum_{i=0}^{P} a_i \Psi_i(\xi), \quad b(\xi) = \sum_{i=0}^{P} b_i \Psi_i(\xi). \tag{24}$$

We want to find the coefficients c_k of the expression

$$c(\xi) = \sum_{k=0}^{P} c_k \Psi_k(\xi) = \sum_{i=0}^{P} \sum_{j=0}^{P} a_i b_j \Psi_i(\xi) \Psi_j(\xi). \tag{25}$$

Following the method introduced in [42], we perform a Galerkin projection onto the polynomial orthogonal basis and use the orthogonality of the basis discussed in the previous section. Then the expression of the coefficients can be found as

$$c_k = \sum_{i=0}^{P} \sum_{j=0}^{P} \frac{\langle \Psi_i \Psi_j \Psi_k \rangle}{\langle \Psi_k^2 \rangle} a_i b_j, \tag{26}$$

where the expectation value $\langle\cdot,\cdot\rangle$ can be evaluated by any numerical integration rule.

Next, we consider a general non-linear function $g(x,\epsilon)$, where ϵ is the random porosity. We need to express this function as

$$g(\mathbf{x},\epsilon)=\sum_{i=0}^{P} g_i\Psi_i, \tag{27}$$

where g_i is the expansion coefficient onto the polynomial basis and the porosity $\epsilon(\mathbf{x},\omega)$ is written here based on the K–L expansion as follows:

$$\epsilon(\mathbf{x},\omega)=\bar{\epsilon}(\mathbf{x})+\sum_{i=1}^{M}\sqrt{\lambda_i}f_i(\mathbf{x})\xi_i(\omega)=\sum_{i=0}^{P}\epsilon_i(\mathbf{x})\Psi_i(\omega). \tag{28}$$

Here, $\epsilon_0(\mathbf{x})=\bar{\epsilon}(\mathbf{x})$, $\epsilon_i(\mathbf{x})=\sqrt{\lambda_i}f_i(\mathbf{x})$, for $i=1,\ldots,M$ and $\epsilon_i(\mathbf{x})=0$, for $i>M$. This is because the first $M+1$ term Hermite polynomials are just $\Psi_0=1,\Psi_1=\xi_1(\omega),\ldots,\Psi_M=\xi_M(\omega)$. By writing the K–L expansion as Eq. (28) instead of Eq. (16), it is easy to formulate and perform the polynomial chaos calculations. Using the same method as before (i.e., performing a Galerkin projection onto each basis element), we can obtain from Eq. (27) the following:

$$\left\langle g\left(\mathbf{x},\sum_{i=0}^{P}\epsilon_i\Psi_i\right),\Psi_j\right\rangle=g_j\langle\Psi_j^2\rangle. \tag{29}$$

Thus, we obtain

$$g_j=\frac{\langle g(\mathbf{x},\sum_{i=0}^{P}\epsilon_i\Psi_i),\Psi_j\rangle}{\langle\Psi_j^2\rangle}. \tag{30}$$

This expression may be evaluated using quadrature rule as discussed in [43] or a non-quadrature-based approach such as the integration, Taylor series and sampling approach discussed in [42]. Here, we employ a Monte-Carlo based sampling approach based on the Latin-Hypercube sampling (LHS) strategy [44]. In this case, we first generate samples of uncorrelated standard normal variables $\boldsymbol{\xi}$ using LHS. The idea of LHS is to subdivide the stochastic support space of the joint PDF of $\boldsymbol{\xi}$ into N subintervals along each stochastic dimension and to ensure that one sample of $\boldsymbol{\xi}$ lies in each subinterval. For each sample, we then calculate the value of the integrand in the numerator of Eq. (30). Summing all the values, the expectation value $\langle\cdot,\cdot\rangle$ is just the arithmetic mean of these realizations. Also, the value of $\langle\Psi_j^2\rangle$ can be pre-computed using quadrature rule.

4.2. GPCE-based formulation

By now, we have developed all the tools we need to formulate natural convection in random porous media. In the stochastic natural convection problem, the input uncertainties are due to the Gaussian random field of porosity.

Note that since there are non-linear functions of $\epsilon(\mathbf{x},\omega)$ in the governing equation (1), we need to first express them in the polynomial basis using the method discussed in the previous section:

$$\frac{1}{\epsilon(\mathbf{x},\omega)}=\sum_{i=0}^{P}\hat{\epsilon}_i\Psi_i, \tag{31}$$

$$\frac{(1-\epsilon(\mathbf{x},\omega))^2}{\epsilon(\mathbf{x},\omega)^2}=\sum_{i=0}^{P}\bar{\epsilon}_i\Psi_i, \tag{32}$$

$$\frac{1-\epsilon(\mathbf{x},\omega)}{\epsilon(\mathbf{x},\omega)^2}=\sum_{i=0}^{P}\tilde{\epsilon}_i\Psi_i, \tag{33}$$

where P is the number of expansion terms determined by the stochastic dimension and expansion order as in Eq. (23).

Thus, the stochastic problem is to find the stochastic functions that describe the velocity field $\boldsymbol{v}(\boldsymbol{x},t,\omega):D\times[0,T]\times\Omega\to\mathbb{R}^d$, the pressure field $p(\boldsymbol{x},t,\omega):D\times[0,T]\times\Omega\to\mathbb{R}$ and the temperature field $\theta(\boldsymbol{x},t,\omega):D\times[0,T]\times\Omega\to\mathbb{R}$, such that the following equations are satisfied:

$$\begin{aligned}\frac{\partial\boldsymbol{v}(\boldsymbol{x},t,\omega)}{\partial t}+\frac{\boldsymbol{v}(\boldsymbol{x},t,\omega)}{\epsilon(\boldsymbol{x},t,\omega)}\cdot\nabla\boldsymbol{v}(\boldsymbol{x},t,\omega)=&-\frac{Pr}{Da}\frac{(1-\epsilon(\boldsymbol{x},t,\omega))^2}{\epsilon(\boldsymbol{x},t,\omega)^2}\boldsymbol{v}(\boldsymbol{x},t,\omega)-\frac{1.75\|\boldsymbol{v}(\boldsymbol{x},t,\omega)\|(1-\epsilon(\boldsymbol{x},t,\omega))}{(150Da)^{1/2}\epsilon(\boldsymbol{x},t,\omega)^2}\boldsymbol{v}(\boldsymbol{x},t,\omega)\\&+Pr\nabla^2\boldsymbol{v}(\boldsymbol{x},t,\omega)-\epsilon(\boldsymbol{x},t,\omega)\nabla p(\boldsymbol{x},t,\omega)-\epsilon(\boldsymbol{x},t,\omega)PrRa\theta(\boldsymbol{x},t,\omega)\mathbf{e}_g,\end{aligned} \tag{34}$$

$$\nabla\cdot\boldsymbol{v}(\boldsymbol{x},t,\omega)=0, \tag{35}$$

$$\frac{\partial\theta(\boldsymbol{x},t,\omega)}{\partial t}+\boldsymbol{v}(\boldsymbol{x},t,\omega)\cdot\nabla\theta(\boldsymbol{x},t,\omega)=\nabla^2\theta(\boldsymbol{x},t,\omega). \tag{36}$$

Since the input uncertainty is taken as a Gaussian random field, we use Hermite polynomials to represent the solution:

$$\boldsymbol{v}(\boldsymbol{x},t,\omega)=\sum_{i=0}^{P}\boldsymbol{v}_i(\boldsymbol{x},t)\Psi_i(\xi),\quad p(\boldsymbol{x},t,\omega)=\sum_{i=0}^{P}p_i(\boldsymbol{x},t)\Psi_i(\xi),$$
$$\theta(\boldsymbol{x},t,\omega)=\sum_{i=0}^{P}\theta_i(\boldsymbol{x},t)\Psi_i(\xi),\quad \boldsymbol{\pi}(\boldsymbol{x},t,\omega)=\sum_{i=0}^{P}\boldsymbol{\pi}_i(\boldsymbol{x},t)\Psi_i(\xi). \tag{37}$$

Substitution of Eqs. (28), (31)–(33) and (37) into the stabilized second-order projection method formulation Eqs. (7) and (10)–(13), results in the following:

$$\begin{aligned}&\frac{1}{\Delta t}\sum_{i=0}^{P}(\boldsymbol{v}_i^{n+1/2}-\boldsymbol{v}_i^{n})\Psi_i+\sum_{i=0}^{P}\sum_{j=0}^{P}\sum_{l=0}^{P}\hat{\epsilon}_l(2\boldsymbol{v}_i^{n}\cdot\nabla\boldsymbol{v}_j^{n}-\boldsymbol{v}_i^{n-1}\cdot\nabla\boldsymbol{v}_j^{n-1})\Psi_i\Psi_j\Psi_l\\&\quad=-\frac{Pr}{Da}\sum_{i=0}^{P}\sum_{j=0}^{P}\bar{\epsilon}_i(2\boldsymbol{v}_j^{n}-\boldsymbol{v}_j^{n-1})\Psi_i\Psi_j+Pr\sum_{i=0}^{P}\nabla^2(\boldsymbol{v}_i^{n+1/2})\Psi_i-\frac{1.75\|\boldsymbol{v}^n\|}{(150Da)^{1/2}}\sum_{i=0}^{P}\sum_{j=0}^{P}\tilde{\epsilon}_i(2\boldsymbol{v}_j^{n}-\boldsymbol{v}_j^{n-1})\Psi_i\Psi_j\\&\qquad-\sum_{i=0}^{P}\sum_{j=0}^{P}\epsilon_i\nabla p_j^{n}\Psi_i\Psi_j-PrRa\sum_{i=0}^{P}\sum_{j=0}^{P}\epsilon_i\theta_j^{n}\Psi_i\Psi_j\mathbf{e}_g,\end{aligned} \tag{38}$$

$$(\Delta t+\tau)\nabla^2\sum_{i=0}^{P}p_i^{n+1}\Psi_i=\Delta t\sum_{i=0}^{P}\nabla^2p_i^{n}\Psi_i+\sum_{i=0}^{P}\nabla\cdot\boldsymbol{v}_i^{n+1/2}\Psi_i+\tau\sum_{i=0}^{P}\nabla\cdot\boldsymbol{\pi}_i^{n}\Psi_i, \tag{39}$$

$$\sum_{i=0}^{P}\boldsymbol{\pi}_i^{n+1}\Psi_i=\sum_{i=0}^{P}\nabla p_i^{n+1}\Psi_i, \tag{40}$$

$$\frac{1}{\Delta t}\sum_{i=0}^{P}(\boldsymbol{v}_i^{n+1}-\boldsymbol{v}_i^{n+1/2})\Psi_i+\sum_{i=0}^{P}\nabla p_i^{n+1}\Psi_i-\sum_{i=0}^{P}\nabla p_i^{n}\Psi_i=0, \tag{41}$$

$$\frac{1}{\Delta t}\sum_{i=0}^{P}(\theta_i^{n+1}-\theta_i^{n})\Psi_i+\sum_{i=0}^{P}\sum_{j=0}^{P}(2\boldsymbol{v}_i^{n}\cdot\nabla\theta_j^{n}-\boldsymbol{v}_i^{n-1}\cdot\nabla\theta_j^{n-1})\Psi_i\Psi_j=\sum_{i=0}^{P}\nabla^2\theta_i^{n+1}\Psi_i. \tag{42}$$

Then performing a Galerkin projection of each equation by $\langle\cdot,\Psi_k\rangle$ [8,10], and using the orthogonality of the polynomial basis Eq. (19), we obtain

$$\begin{aligned}&\frac{1}{\Delta t}(\boldsymbol{v}_k^{n+1/2}-\boldsymbol{v}_k^{n})+\frac{\langle\Psi_i\Psi_j\Psi_l\Psi_k\rangle}{\langle\Psi_k^2\rangle}\sum_{i=0}^{P}\sum_{j=0}^{P}\sum_{l=0}^{P}\hat{\epsilon}_l(2\boldsymbol{v}_i^{n}\cdot\nabla\boldsymbol{v}_j^{n}-\boldsymbol{v}_i^{n-1}\cdot\nabla\boldsymbol{v}_j^{n-1})\\&\quad=-\frac{Pr}{Da}\sum_{i=0}^{P}\sum_{j=0}^{P}\bar{\epsilon}_i(2\boldsymbol{v}_j^{n}-\boldsymbol{v}_j^{n-1})e_{ijk}-\frac{1.75\|\boldsymbol{v}^n\|}{(150Da)^{1/2}}\sum_{i=0}^{P}\sum_{j=0}^{P}\tilde{\epsilon}_i(2\boldsymbol{v}_j^{n}-\boldsymbol{v}_j^{n-1})e_{ijk}+Pr\nabla^2\boldsymbol{v}_k^{n+1/2}-\sum_{i=0}^{P}\sum_{j=0}^{P}\epsilon_i\nabla p_j^{n}e_{ijk}\\&\qquad-PrRa\sum_{i=0}^{P}\sum_{j=0}^{P}\epsilon_i\theta_j^{n}e_{ijk}\mathbf{e}_g,\end{aligned} \tag{43}$$

$$(\Delta t+\tau_k)\nabla^2p_k^{n+1}=\Delta t\nabla^2p_k^{n}+\nabla\cdot\boldsymbol{v}_k^{n+1/2}+\tau_k\nabla\cdot\boldsymbol{\pi}_k^{n}, \tag{44}$$

$$\boldsymbol{\pi}_k^{n+1}=\nabla p_k^{n+1}, \tag{45}$$

$$\frac{1}{\Delta t}(\boldsymbol{v}_k^{n+1}-\boldsymbol{v}_k^{n+1/2})+\nabla p_k^{n+1}-\nabla p_k^{n}=0, \tag{46}$$

$$\frac{1}{\Delta t}(\theta_k^{n+1}-\theta_k^{n})+\sum_{i=0}^{P}\sum_{j=0}^{P}(2\boldsymbol{v}_i^{n}\cdot\nabla\theta_j^{n}-\boldsymbol{v}_i^{n-1}\cdot\nabla\theta_j^{n-1})e_{ijk}=\nabla^2\theta_k^{n+1}, \tag{47}$$

where $e_{ijk}=\frac{\langle\Psi_i\Psi_j\Psi_k\rangle}{\langle\Psi_k^2\rangle}$, $k=0,1,\ldots,P$. This results in $(P+1)(3d+2)$ decoupled deterministic equations.

Remark 2. In Eq. (43), it is time consuming to evaluate the fourth-order product term $\frac{2}{\langle\Psi_k^2\rangle}\sum_{i=0}^{P}\sum_{j=0}^{P}\sum_{l=0}^{P}\hat{\epsilon}_l\boldsymbol{v}_i^{n}\cdot\nabla\boldsymbol{v}_j^{n}\langle\Psi_i\Psi_j\Psi_l\Psi_k\rangle$ directly using the method discussed in Section 4.1. To simplify this calculation, we introduce an auxiliary random variable as follows:

$$d = \sum_{m=0}^{P} d_m \Psi_m = \sum_{i=0}^{P} \sum_{l=0}^{P} \hat{\epsilon}_l \boldsymbol{\nu}_i^n \Psi_i \Psi_l, \tag{48}$$

such that

$$d_m = \sum_{i=0}^{P} \sum_{l=0}^{P} \hat{\epsilon}_l \boldsymbol{\nu}_i^n e_{\lim}. \tag{49}$$

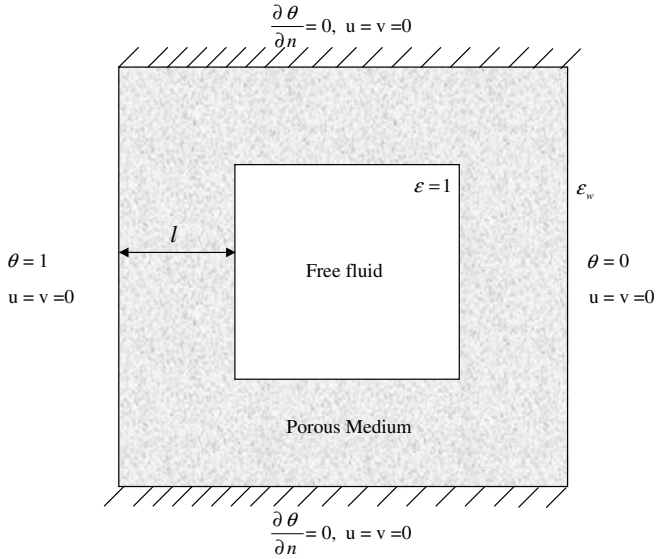

Fig. 1. Schematic of natural convection in a fluid saturated variable porous medium.

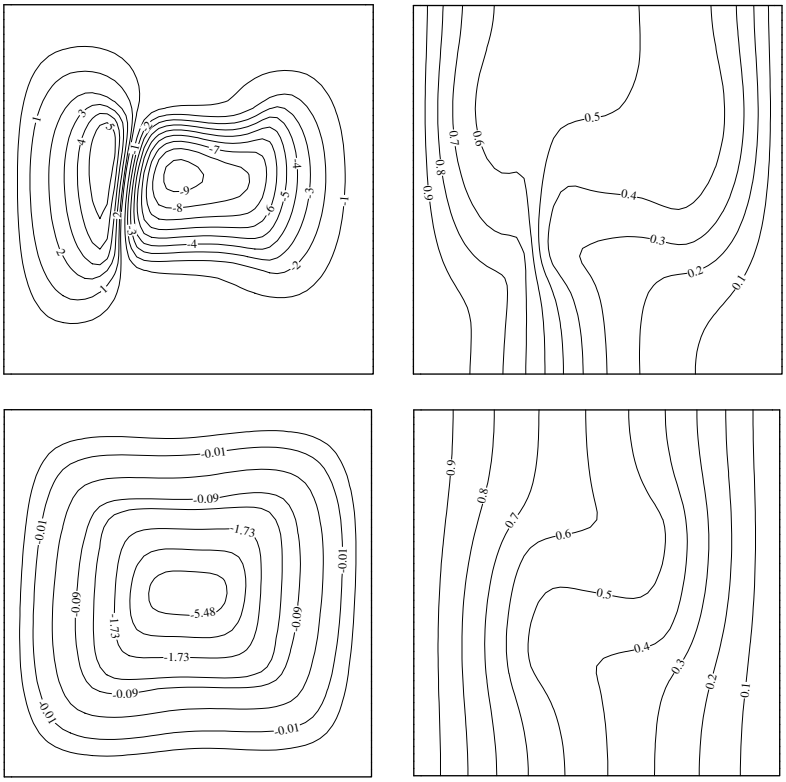

Fig. 2. Comparison of the streamlines (left) and isotherms (right). Top row: first-order projection method. Bottom row: second-order projection method.

So our term of interest can be reduced to $\frac{2}{\langle \Psi_k^2 \rangle} \sum_{j=0}^{P} \sum_{m=0}^{P} d_m \cdot \nabla \boldsymbol{v}_j^n \langle \Psi_j \Psi_m \Psi_k \rangle$. This form is now easier to calculate, since it only evolves third-order product terms.

Remark 3. In the non-linear drag term $-\frac{1.75\|\boldsymbol{v}^n\|}{(150Da)^{1/2}} \sum_{i=0}^{P} \sum_{j=0}^{P} \tilde{\epsilon}_i (2\boldsymbol{v}_j^n - \boldsymbol{v}_j^{n-1}) e_{ijk}$, we assume that the magnitude of the velocity $\|\boldsymbol{v}^n\|$ is determined by the mean velocity $\boldsymbol{v}_0^n$.

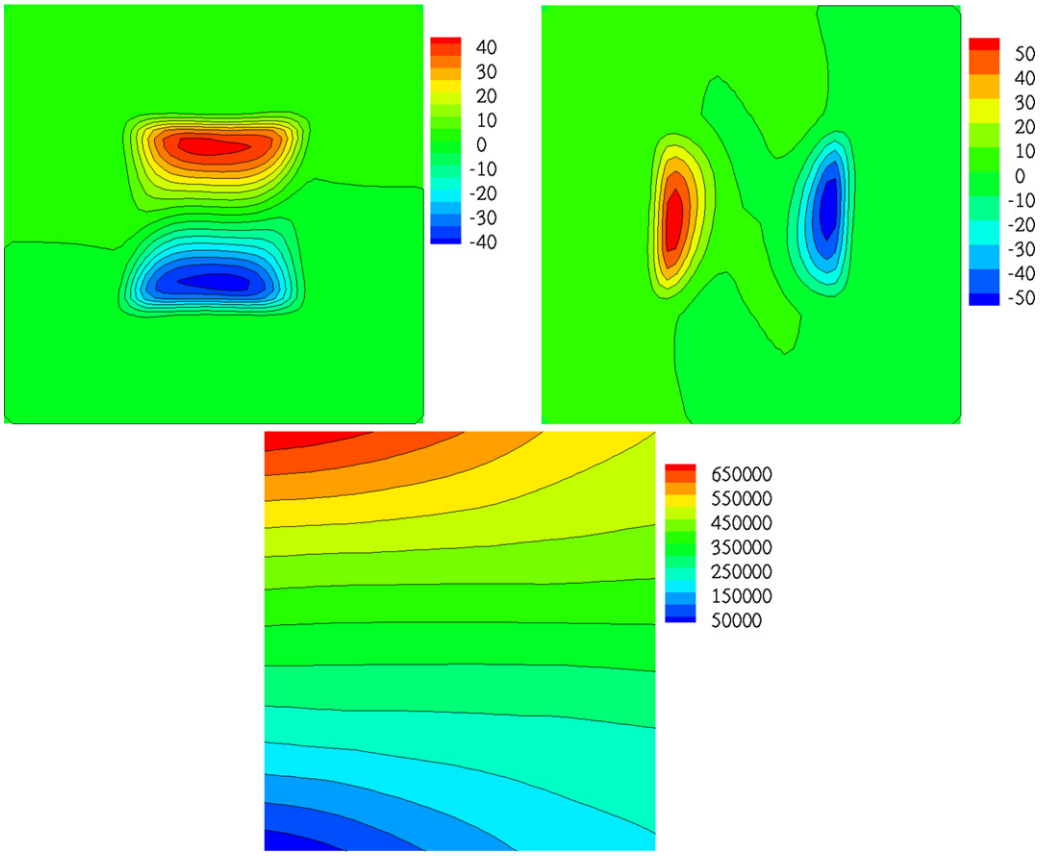

Fig. 3. Contour results obtained with the second-order projection method. Top row: u and v velocity component contours. Bottom row: pressure contours.

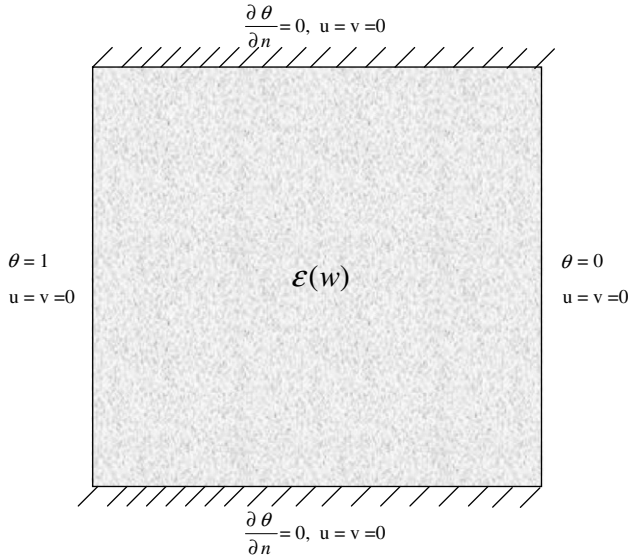

Fig. 4. Schematic of stochastic natural convection in a heterogeneous porous medium.

Remark 4. From Eq. (44), since the PCE terms are decoupled, the stabilized parameter τ is determined by the kth coefficient of the spectral expansion of the velocity components. So we denote it as τ_k to emphasize that it is a function of the kth coefficient $\boldsymbol{v}_k$ according to Eq. (4).

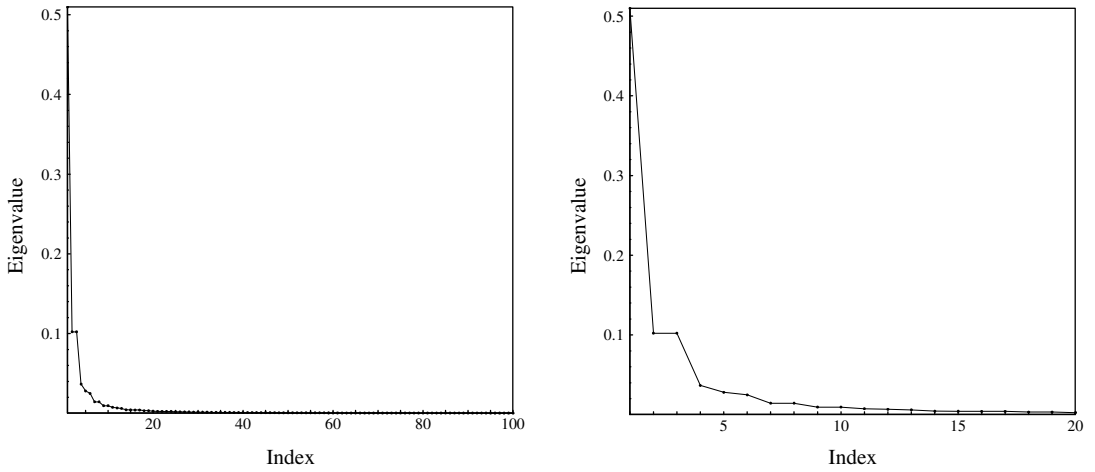

Fig. 5. Eigenspectrum of the correlation kernel (left: first 100 terms; right: first 20 terms).

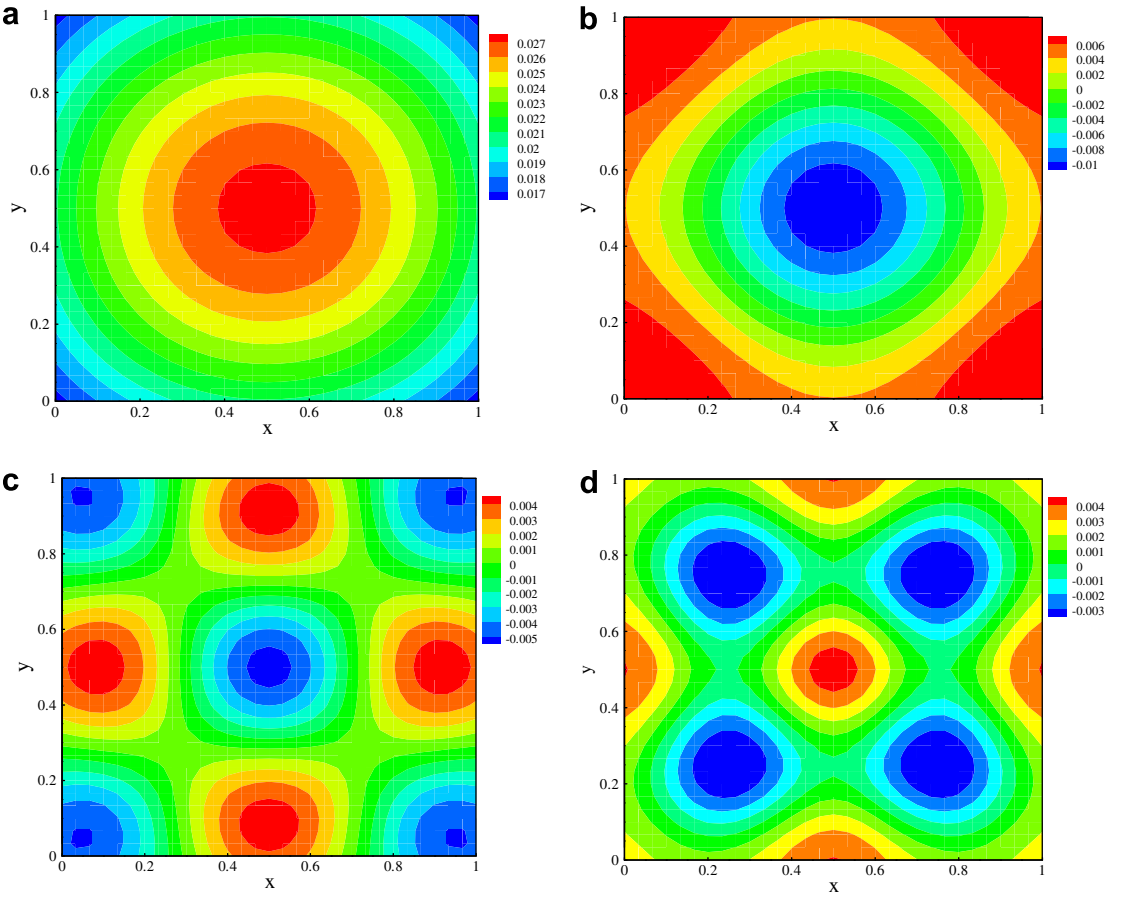

Fig. 6. Eigenmodes of the porosity correlation field: (a) the 1st eigenmode, (b) the 5th eigenmode, (c) the 11th eigenmode and (d) the 14th eigenmode.

Remark 5. For the pressure solution, notice that we impose $p_i(0,0) = 0$ for each polynomial chaos pressure coefficient. The selection of this reference pressure value does not affect the velocity or pressure gradient only resulting to a shift of the pressure solution.

4.3. Spatial discretization

From the formulation of Eqs. (43)–(47), we have moved the randomness into the polynomial chaos basis resulting in a set of deterministic equations. We want to seek the deterministic coefficients of the GPCE expansion. This can be done by any method, such as finite difference and spectral/*hp* element method. Here, we will employ the finite element method to solve the equations.

Let us consider a discretization of the computational domain $\mathcal{D}$ into *Nel* disjoint subdivisions denoted by $\mathcal{D}^{(e)}$. In each of the elements, the finite element basis function is $N(\boldsymbol{x})$. So for each GPCE coefficient in each finite element, we can write

$$\begin{aligned} \boldsymbol{v}_i(\boldsymbol{x},t) &= \sum_{j=1}^{Nbf} \boldsymbol{v}_{ij}(t)N_j(\boldsymbol{x}), \quad p_i(\boldsymbol{x},t) = \sum_{j=1}^{Nbf} p_{ij}(t)N_j(\boldsymbol{x}), \\ \theta_i(\boldsymbol{x},t) &= \sum_{j=1}^{Nbf} \theta_{ij}(t)N_j(\boldsymbol{x}), \quad \boldsymbol{\pi}_i(\boldsymbol{x},t) = \sum_{j=1}^{Nbf} \boldsymbol{\pi}_{ij}(t)N_j(\boldsymbol{x}), \end{aligned} \tag{50}$$

where *Nbf* is the number of basis function in each finite element. So, for example, θ_{ij} denotes the *j*th nodal value of the *i*th GPCE coefficient of temperature in each element. Introducing these expressions into the GPCE formulation and performing a standard Galerkin projection onto the spatial basis functions, one can obtain the final discretized equations.

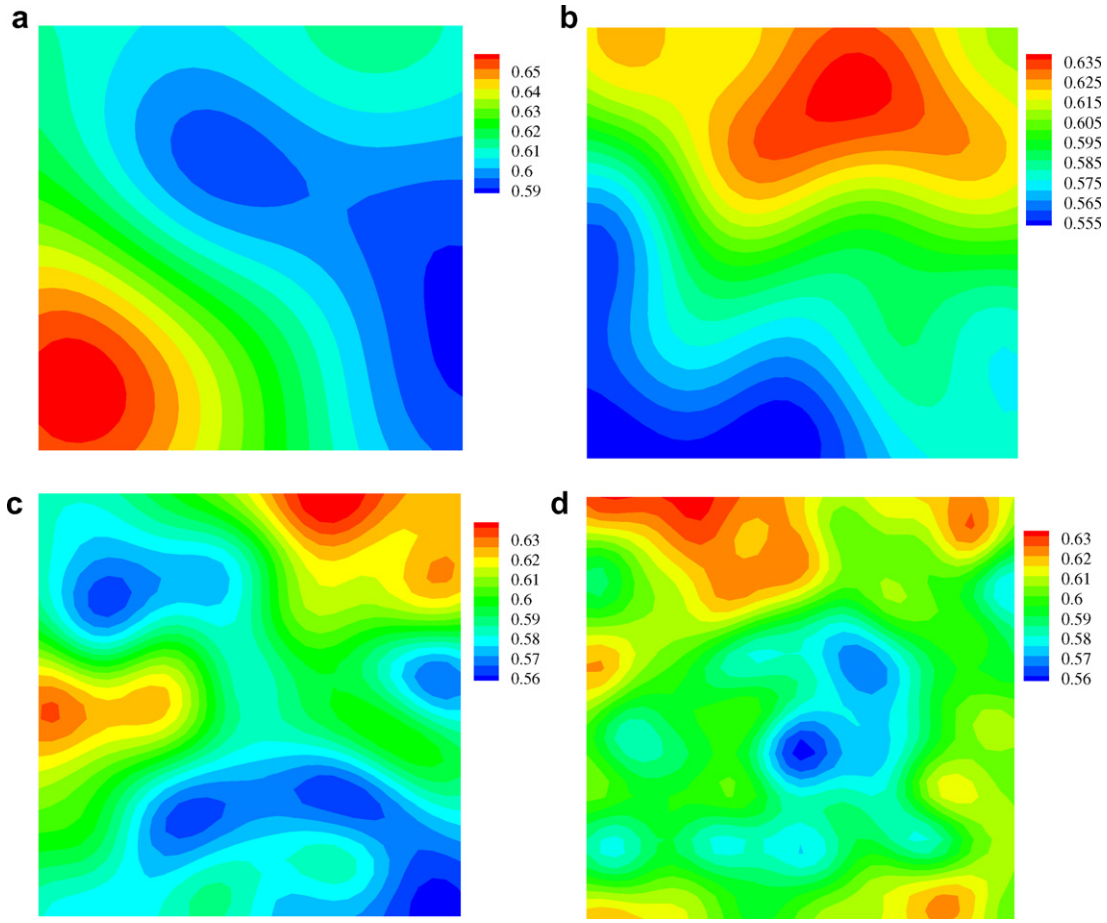

Fig. 7. Realizations of the porosity random field: realization with (a) 10 terms, (b) 20 terms, (c) 50 terms and (d) 100 terms.

5. Numerical examples

Unless otherwise specified, bilinear quadrilateral elements are used for spatial finite element interpolation and Hermite polynomials are used for the GPCE representation of the main field variables (velocity, pressure and temperature). The x and y velocity components in all two-dimensional examples considered here are denoted as u and v, respectively. All calculations are performed using numerical algorithms provided in PETSc. The default Krylov solver was used as the linear solver. All of the quantities considered in the following numerical examples are dimensionless.

5.1. Deterministic natural convection in a fluid saturated variable porosity medium

Let us first consider a benchmark deterministic example as a demonstration of the effectiveness of the pressure stabilized second-order projection formulation. This example considers natural convection in a variable porosity medium (Fig. 1). The computational region is a $[0,1] \times [0,1]$ square domain. The dimensionless length l in Fig. 1 is taken as $l = 0.3$. The wall porosity ϵ_w is taken as 0.4. The porosity increases linearly from 0.4 at the wall to 1.0 (pure liquid) at the core. The Rayleigh number is 1×10^6, Prandtl number is 1.0 and the Darcy number is 6.665×10^{-7}. The problem was solved with a mesh discretization 50×50 and the time step was chosen as 5×10^{-5}. The simulation was run up to non-dimensional time 1.0.

This problem is originated from [1], where the author used a first-order projection method. In [37], the same problem was addressed using a SUPG (streamline upwind Petrov–Galerkin) as well as PSPG (pressure) and DSPG (Darcy) stabilized Petrov–Galerkin formulations with equal-order velocity–pressure finite element interpolation. A second-order projection method without pressure stabilization was also applied for the solution of this problem in [45].

The isotherms and streamline pattern obtained by the first-order and the second-order projection methods are shown in Fig. 2. From this figure, we can see that the results obtained with the two methods are totally different. We argue that the

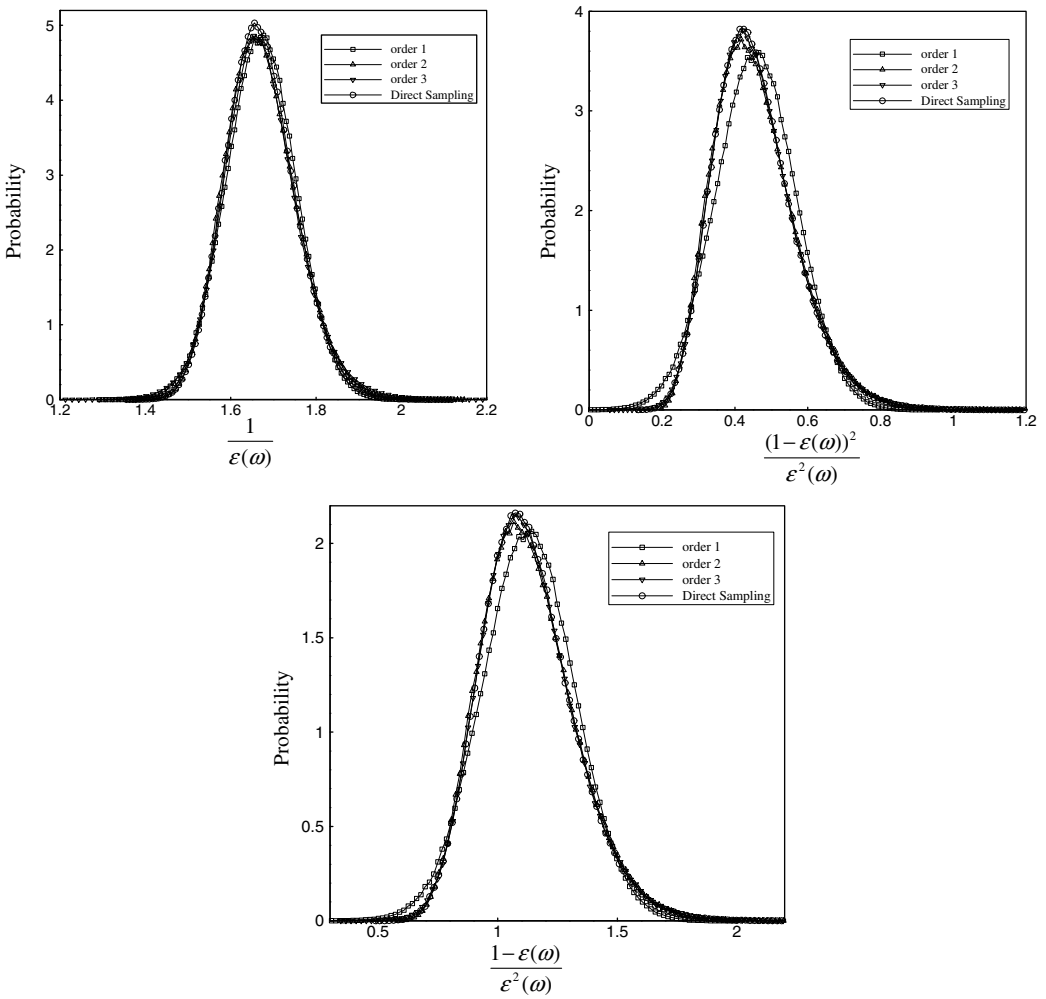

Fig. 8. PDF of non-linear functions as obtained from DS and GPCE expansion at point (0.47, 0.7).

first-order projection method is not applicable to this problem. Indeed from the governing equation (7), we can clearly see that the porosity is part of the pressure gradient term. So the role of pressure here is not just to impose the continuity constraint as is the case in the first-order method. In addition, we can clearly notice that the streamline pattern using the first-order method is not symmetric. However, since the original problem definition is symmetric in velocity and porosity, the symmetry should not be broken despite the temperature boundary conditions. On the other hand, the streamline pattern using the second-order method is approximately symmetric with respect to the center of the region. The authors in [45] also pointed out recently this symmetry issue.

The obtained contours for the velocity components and pressure are shown in Fig. 3. Note that the velocity contour using the second-order scheme is mainly distributed in the free fluid region as it is physically expected. However, the velocity contour in the porous region using the first-order method is the same magnitude as in the free fluid. Furthermore, the pressure contours are quite different between the two methods not only in the shape but also the values.

We also compared the results with those in [37] where a stabilized finite element method was used and the pressure gradient was included in the momentum equation. The isotherms and the maximum value of the streamline are nearly identical with the results obtained with the second-order projection method. However, the solution in [37] is still not symmetric.

From the above discussion, it is clear that the second-order projection method maintains symmetry (regardless of the temperature boundary conditions) and provides the correct flow and thermal patterns for convection in porous media with varying porosity. Now we are ready to extend this idea to the stochastic second-order projection method and solve the stochastic convection problem in random heterogeneous porous media.

5.2. Two-dimensional natural convection in random porous media

A schematic of the problem is shown in Fig. 4. The Rayleigh number is taken as 1×10^4, the Prandtl number is 1.0 and the Darcy number is 7.407×10^{-3}. The problem was solved with a mesh discretization 30×30 on a square domain $[0,1] \times [0,1]$ and time step 1×10^{-3}. The initial condition for velocity and temperature is 0. The problem was run up until steady-state.

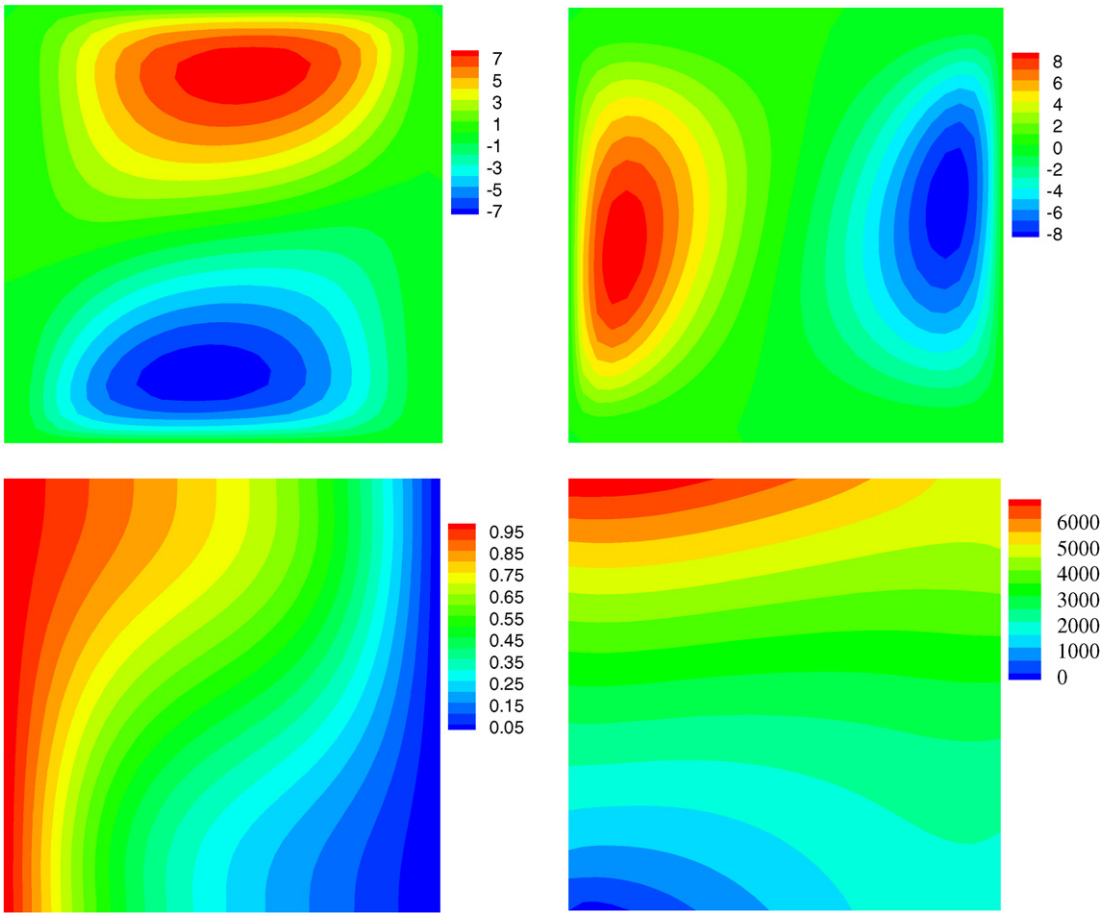

Fig. 9. Mean values of the variables (top left: u velocity component, top right: v velocity component; bottom left: temperature, bottom right: pressure).

The input uncertainty comes from the porosity. The mean porosity is taken as 0.6 and an exponential covariance kernel is assumed as follows:

$$R_{hh}(\mathbf{x},\mathbf{y}) = \sigma^2 \exp\left(-\frac{r}{b}\right), \tag{51}$$

where r is the distance between two spatial points and b is the correlation length. An exponential correlation kernel is the result of a bilateral auto-regression and is most commonly used for describing a second-order stochastic process [8,10]. Higher correlation length would lead to a rapid decay of the eigenvalues in the K–L expansion, i.e., in a reduction in the stochastic input dimension. For this example, the correlation length is taken as $b = 0.7$, and the standard deviation as $\sigma = 1$. The coefficient of variation, which is defined as the standard deviation to the mean of the stochastic process, is 166.67%.

The computed eigenvalues of the correlation function are shown in Fig. 5. From the figure on the right, it is seen that the first six eigenvalues correspond to 95% of the porosity eigenspectrum. Thus, we consider the porosity to be expanded using six terms in the K–L expansion and the stochastic dimension is taken as 6. Examples of eigenmodes $\sqrt{\lambda_i} f_i(\mathbf{x})$ are shown in Fig. 6.

It should be noted that the K–L expansion provides an efficient way for random field generation. Once the eigenmodes are found, a realization of the porosity can be computed simply by independently sampling n standard Gaussian random variables and then computing the value using Eq. (14), where n is the number of terms in the K–L expansion needed to generate realizations with a given accuracy. These realizations can be used with Monte-Carlo simulation to allow comparison with the results of the GPCE methodology. From the left figure in Fig. 5, it is seen that the first 20 terms represent $\sim 99\%$ of the porosity eigenspectrum. It will be shown in Section 5.2.5 that MC simulation with six terms in the K–L expansion leads to approximately the same solutions as when using 20 terms. Thus, the assumption of a six-dimensional stochastic porosity in the

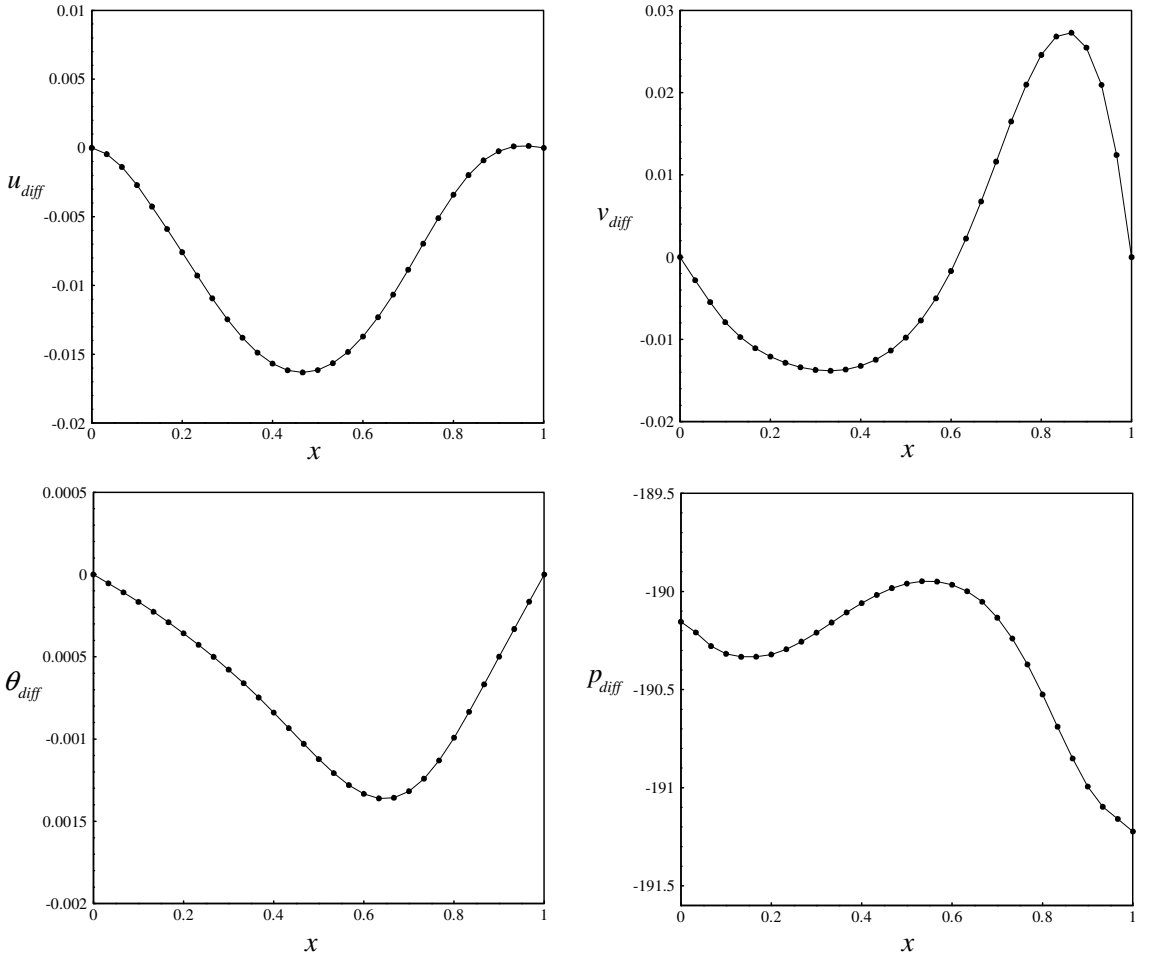

Fig. 10. Differences between the mean and deterministic solution along $y = 0.7$ (top left: u velocity component, top right: v velocity component; bottom left: temperature, bottom right: pressure).

GPCE approach is adequate for this problem. Realizations of the porosity random field with different number of terms in the K–L expansion are shown in Fig. 7.

The optimal order of the GPCE expansion is determined a priori. After computing the K–L expansion of the porosity $\epsilon(\mathbf{x}, \omega)$, we can evaluate the coefficients of the GPCE expansion for the three non-linear functions given in the right-hand side of Eqs. (31)–(33) using the method discussed in Section 4.1. The optimal order is determined such that the GPCE

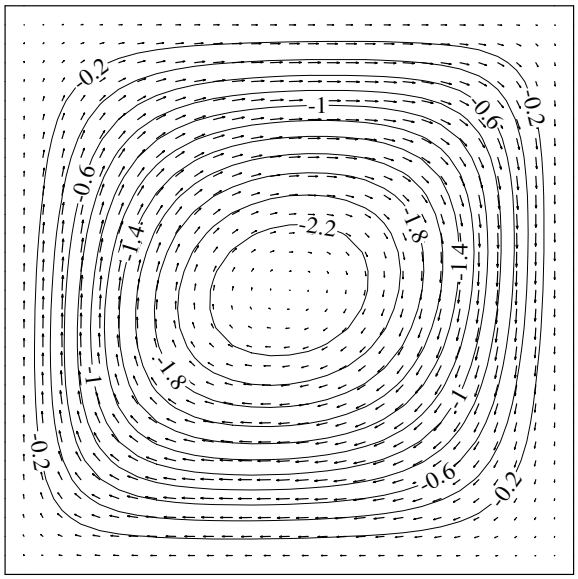

Fig. 11. Mean velocity vectors and streamlines.

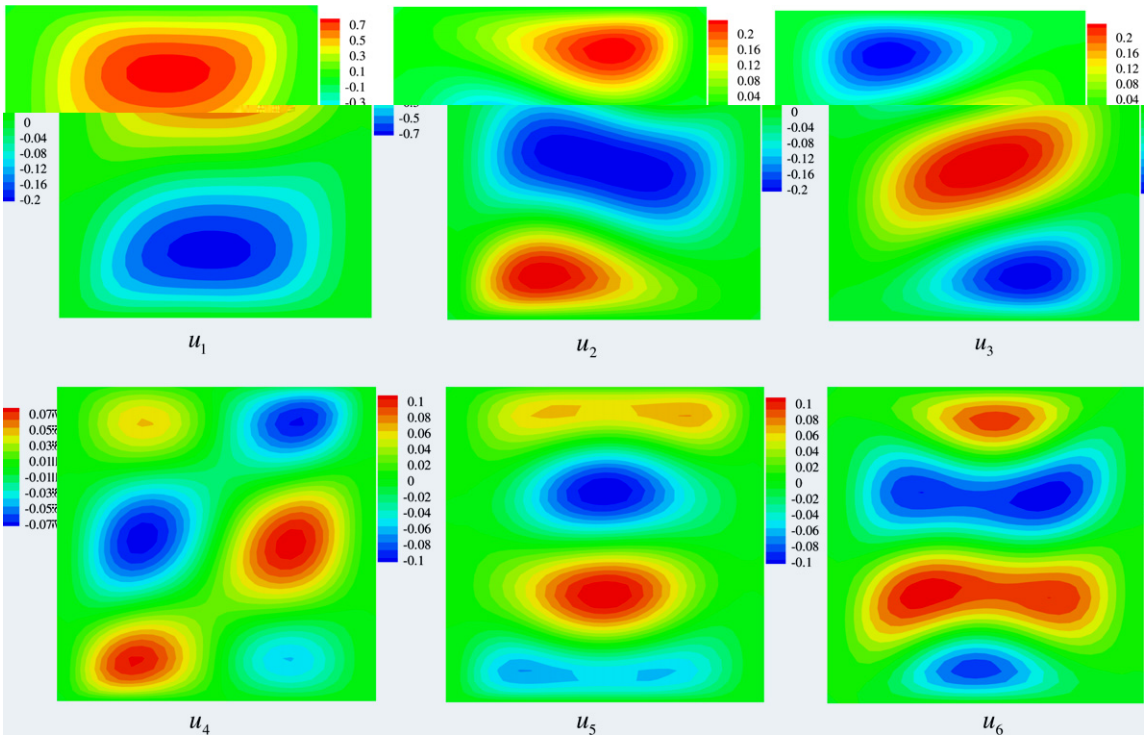

Fig. 12. First-order modes of the *u* velocity component.

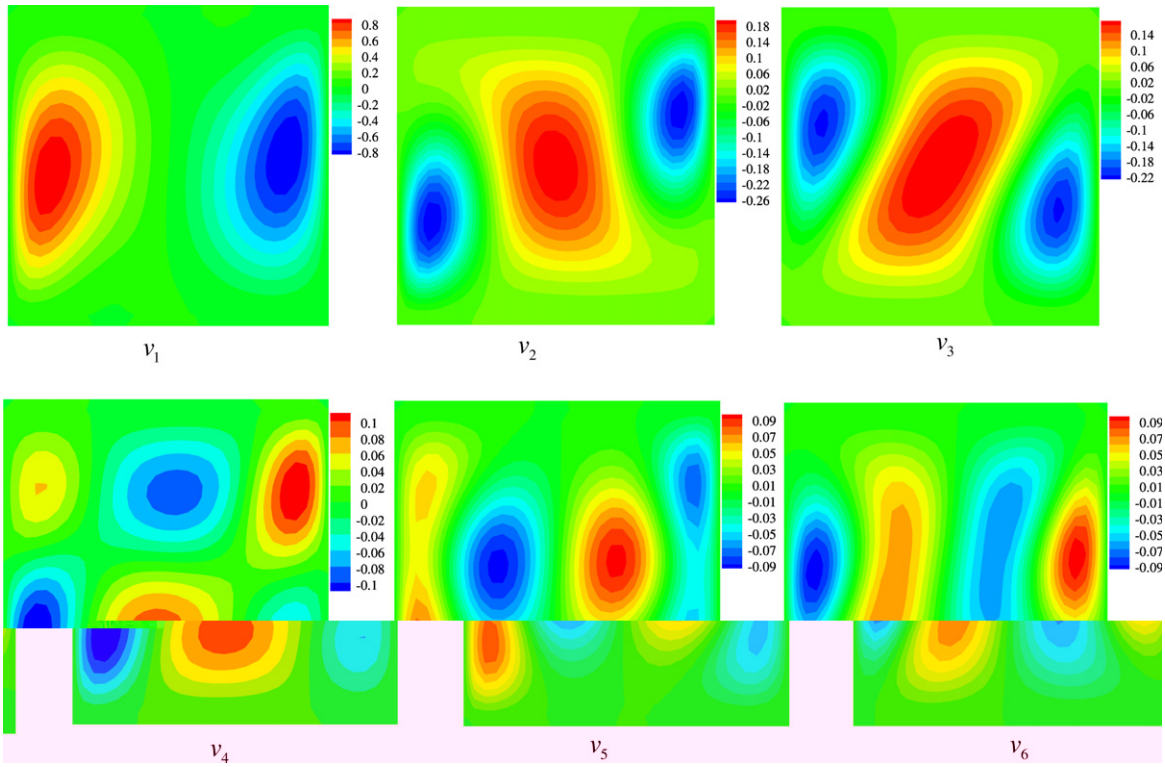

Fig. 13. First-order modes of the v velocity component.

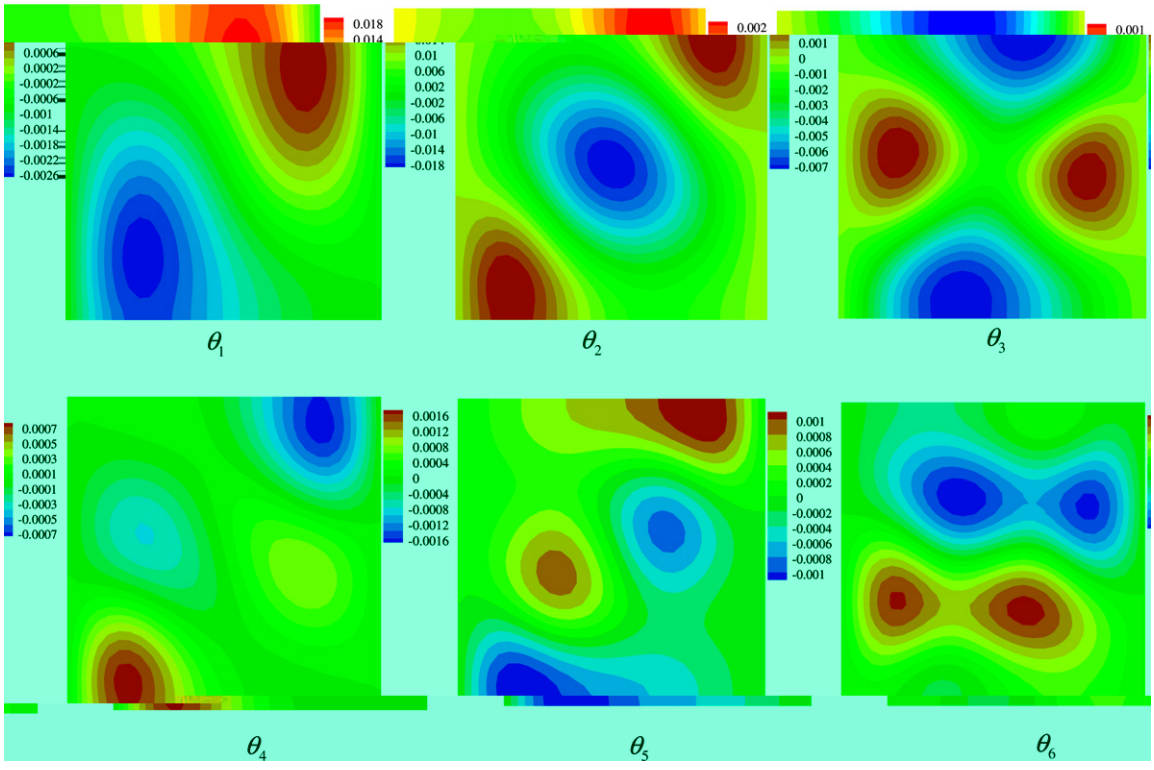

Fig. 14. First-order modes of temperature.

expansion can accurately represent the PDFs of these non-linear functions. We then generate the realizations from the calculated expansion on the right-hand side of Eqs. (31)–(33) and plot the histogram of all the realizations to obtain the PDFs. We compare the results with the "direct sampling" (DS) approach, where the PDF of the functions in Eqs. (31)–(33) is obtained by sampling ξ_i in Eq. (28) from the independent standard normal distribution, then substitute the random variables ξ_i into the K–L expansion Eq. (28) to obtain one sample of ϵ, finally calculate the value of each non-linear function in Eqs. (31)–(33) and plot the histogram of all the realizations to obtain the PDFs. The results are shown in Fig. 8 at point (0.47, 0.70). It is clearly seen that a second-order GPCE expansion is enough to capture the input uncertainty. Thus, we choose a six-dimension second-order GPCE expansion to represent the solution process. For this spectral resolution, $P = 27$, which results in a total of 28 modes.

5.2.1. The zeroth-order mode: mean solution

In this section, we first discuss the behavior of the mean solution (see Fig. 9). At first note that the mean values of the temperature and velocity component distributions differ from the corresponding deterministic predictions. The differences between the mean and the deterministic solutions are shown in Fig. 10.

From these figures, as expected, we can see that the uncertainty in porosity affects the magnitude of velocity much more than it affects the temperature. Also, note that, for the u velocity component, there is a large variation along the center line, while for v and temperature, the large variations occur near the vertical walls. These large differences suggest large standard deviation in these regions, which is consistent with the contour plots of the standard deviation shown in Section 5.2.4. Fig. 11 plots the mean velocity vectors and some streamlines.

5.2.2. The first-order mode behavior

The first-order modes are shown in Figs. 12–14. They correspond to the polynomials $\Psi_k = \xi_k$ for $k = 1, 2, \ldots, 6$. These modes reflect the linear response of the stochastic field and fluctuations around the mean. As mentioned before, since the

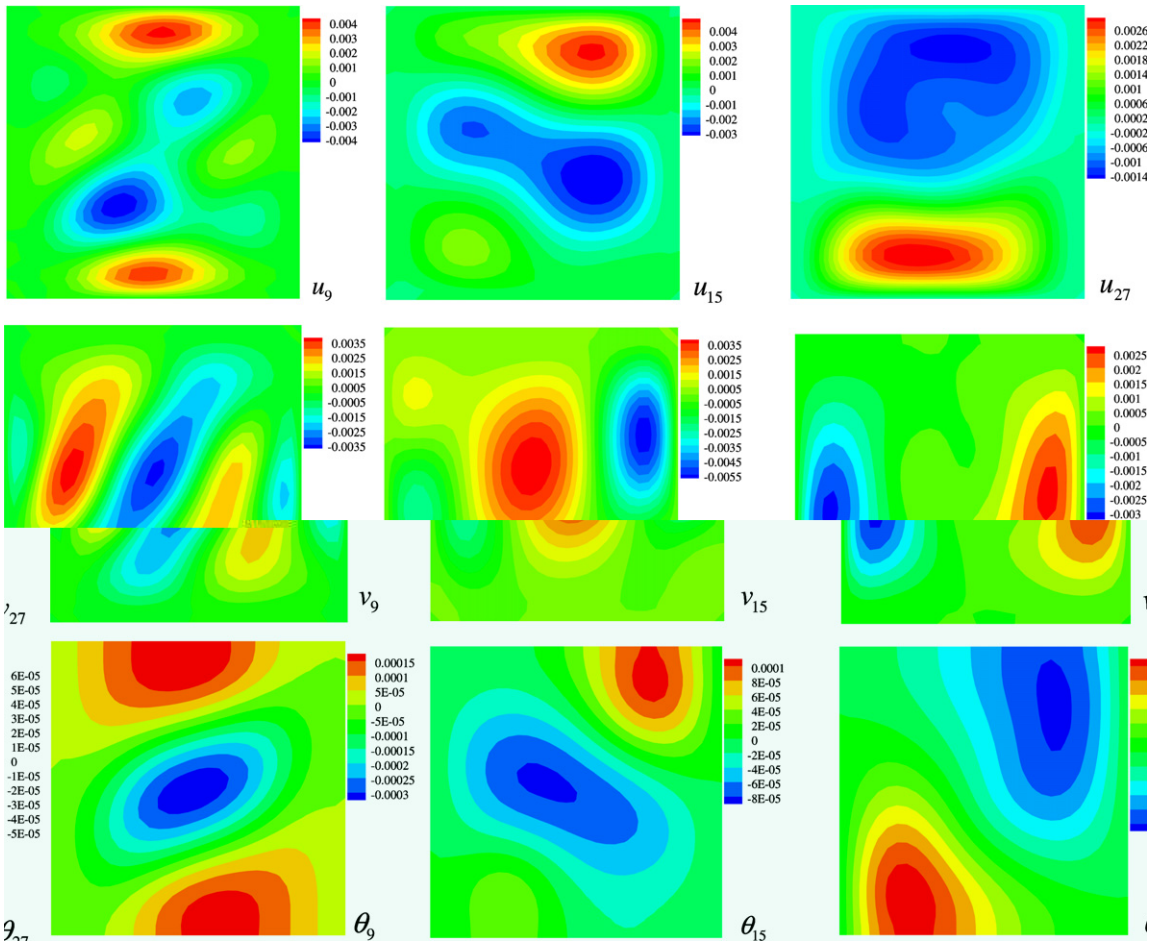

Fig. 15. The second-order modes of the solution (top row: u velocity component; middle row: v velocity component; bottom row: temperature).

input uncertainty of the porosity field is propagated through the momentum equation, the contours of the velocity components have similar patterns as the K–L eigenmodes shown in Fig. 6.

Now let us examine the first-order modes of the temperature. The first mode θ_1 exhibits a different pattern from the mean temperature and it is similar to the standard deviation pattern as shown later in Fig. 16. This mode is dominant and contributes mostly to the uncertainty of the temperature. One can also note that the fluctuations of temperature of the other modes are governed by the patterns of the corresponding flow modes in the cavity. Thus, although the input uncertainty affects mainly the flow in the cavity, it also propagates through the thermal transport equation to cause the temperature fluctuation. Finally, note that the contour values of the first-order modes of temperature and velocity components are at least one order of magnitude lower than the corresponding mean values.

5.2.3. The second-order mode behavior

The second-order modes correspond to the polynomials Ψ_k for $k = 7, 8, \ldots, 27$. Some of them are shown in Fig. 15. They capture the strong non-linear dependence of the solution process. These results are more difficult to interpret than the first-order modes. The pattern of the contours are very complex, some of which are localized along the wall, while others are extended through the whole domain. However, it is still clear that the fluctuation of the temperature is governed by the corresponding velocity field. The values of the second-order modes are at least one order of magnitude lower than the first-order modes, which illustrates the fast convergence of the polynomial chaos expansions.

5.2.4. Higher-order moments and probability density functions

When the coefficients of the polynomial chaos expansion are computed, we obtain an approximate solution in the stochastic support space. It is now rather easy to extract higher-order statistics from this solution through sampling strategies. As an example, Fig. 16 plots the standard deviation of the velocity, temperature and pressure fields. The effect of the uncertainty in porosity is to change the convective pattern in the domain. The PDFs are plotted at the point (0.53, 0.73) that has a high standard deviation in u (see Fig. 16). The variables at this point were sampled randomly 500,000 times from the

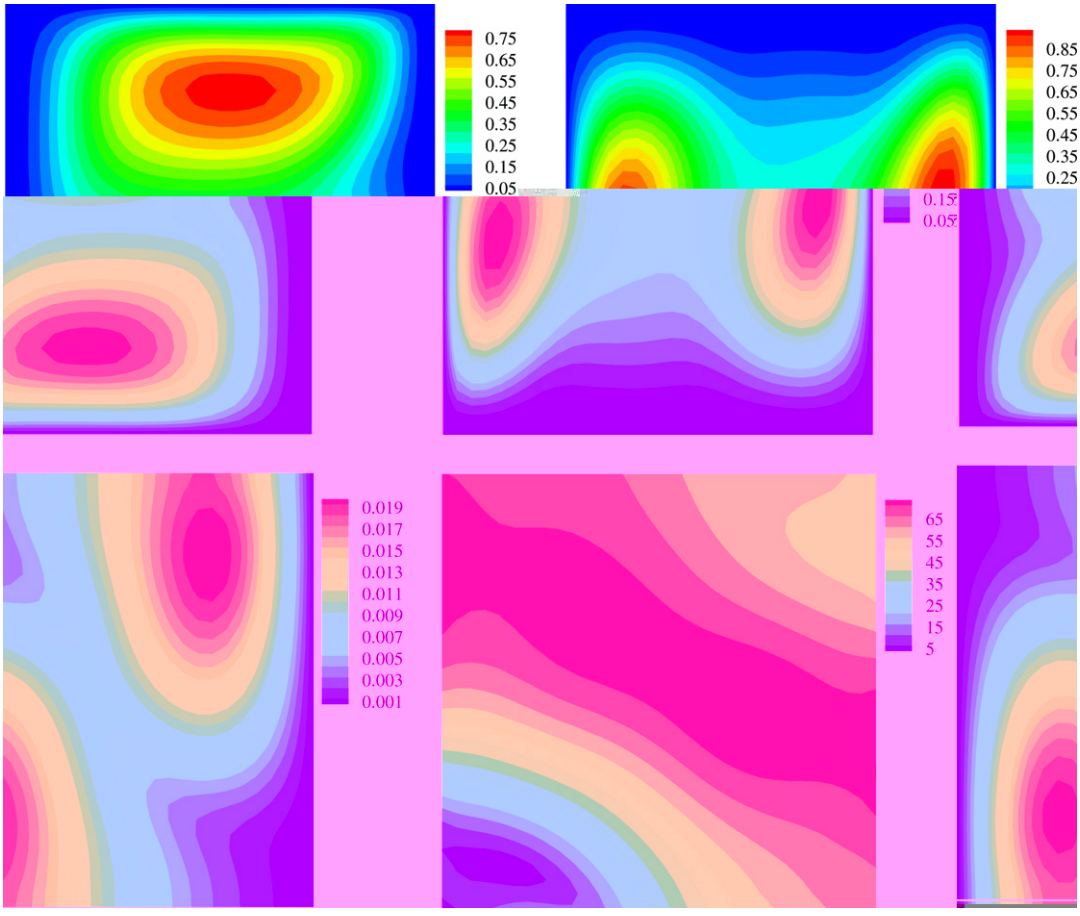

Fig. 16. The standard deviation of the fields (top left: u velocity component, top right: v velocity component; bottom left: temperature, bottom right: pressure).

six-dimensional stochastic space and the corresponding PDFs were computed from the histogram distributions. They are shown in Fig. 17. The results are compared with Monte-Carlo (MC) simulation, where 50,000 samples are generated.

It is seen that the results compare quite well with the MC results. This partially verifies the second-order projection method. Note that the computed range of possible values of each variable shown is quite large. Also note that the range of the v velocity component can change from a negative to a positive value.

5.2.5. Comparison with other solution strategies

In order to validate the present GPCE model, we compare the mean and standard deviation with the results obtained from the sparse grid collocation method [36] and the Monte-Carlo method. The results are shown in Figs. 18 and 19. Convergence study has been conducted when using the MC method. The results show that 50,000 samples are enough to capture all the statistics. Sample statistics of the variables, i.e., the mean and the standard deviation, are computed from the realizations. Recall that 20 terms are used in the K–L expansion in these MC results, while we have limited the number of independent random variables in the GPCE expansion to 6. We also test for convergence when using the collocation method. A level 5 collocation, which corresponds to 4865 collocation points, is enough to interpolate the solutions in the stochastic space. The SSFEM solutions are shown to be in an excellent agreement with the other two methods in both the mean and standard deviation. This verifies the accuracy of the stochastic second-order projection finite element method.

The above results also demonstrate that the reduced dimensionality used in the GPCE expansion was sufficient in representing the propagation of porosity uncertainty in the temperature and velocity fields. To further emphasize this point, we also compare the results with the solution obtained using 100 terms in the K–L expansion in the Monte-Carlo simulation, which are shown in Fig. 20. The results again compare very well with the GPCE and collocation methods. So it is seen that

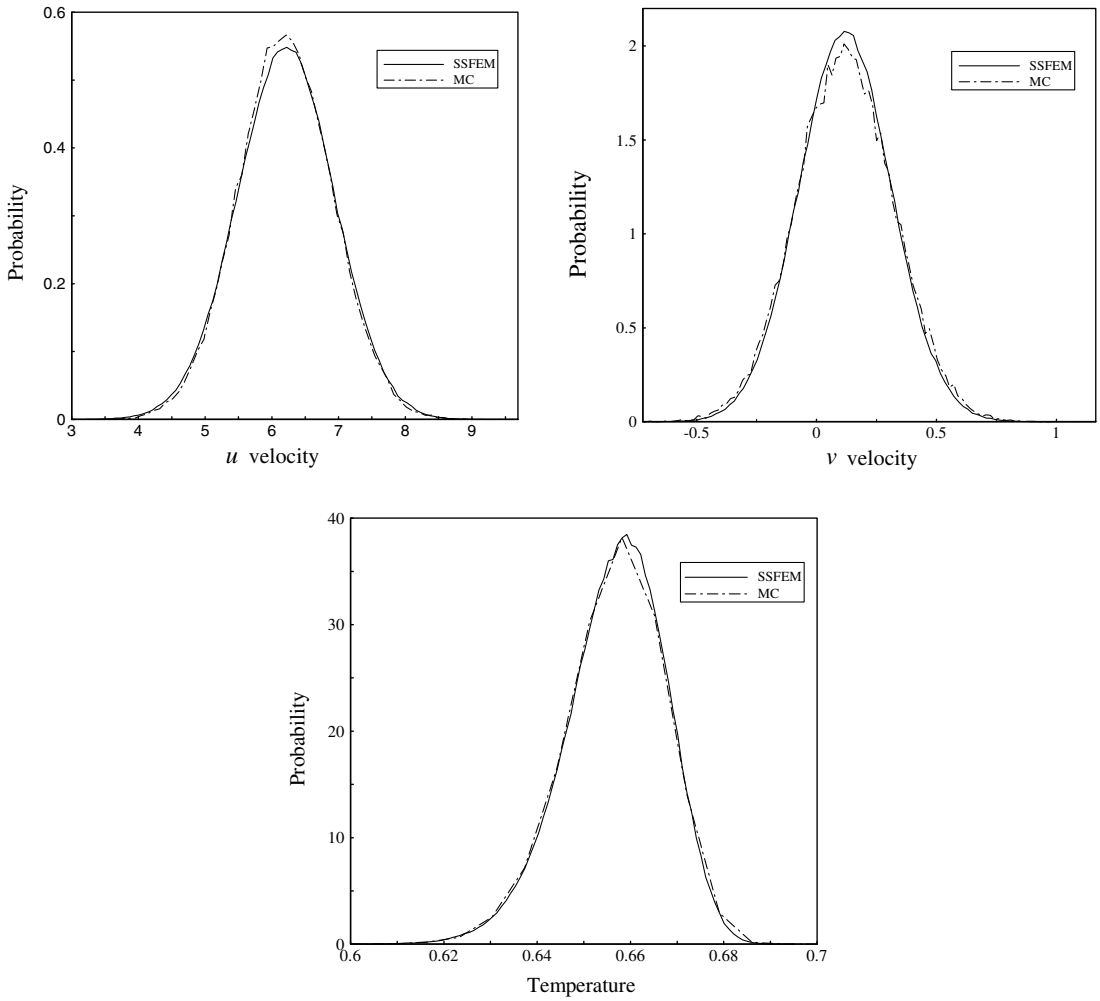

Fig. 17. Probability density function for the variables at point (0.53, 0.73). The MC results shown here have been obtained with 20 terms in the K–L expansion.

using small number of terms in GPCE can capture the strong non-linear fluctuation in the random porosity field. It should be noted that, as mentioned before, the number of terms needed in the K–L expansion depends strongly on the correlation scale. Here, we chose a reasonable correlation length such that small number of terms (six) can represent most of the energy in the porosity eigenspectrum. So the GPCE results are nearly the same as the MC results where more K–L expansion terms are included than in the GPCE. However, when the correlation length is small compared to the domain size, more terms (higher stochastic dimension) will be needed in order to obtain the same results as those of the MC method. Due to the curse of dimensionality issue in GPCE, it is computationally expensive to deal with high-stochastic dimension problems. Therefore, caution should be given when using this method to solve problems with small correlation length in porosity. A sufficient high number of terms is needed in GPCE in order to obtain an accurate solution for such problems.

Finally, we note that the total computation time for SSFEM is 7230 min, which is faster than MC by at least an order of magnitude. On the other hand, the simulation time for the sparse grid collocation method was 5180 min which is a little bit faster than the SSFEM method.

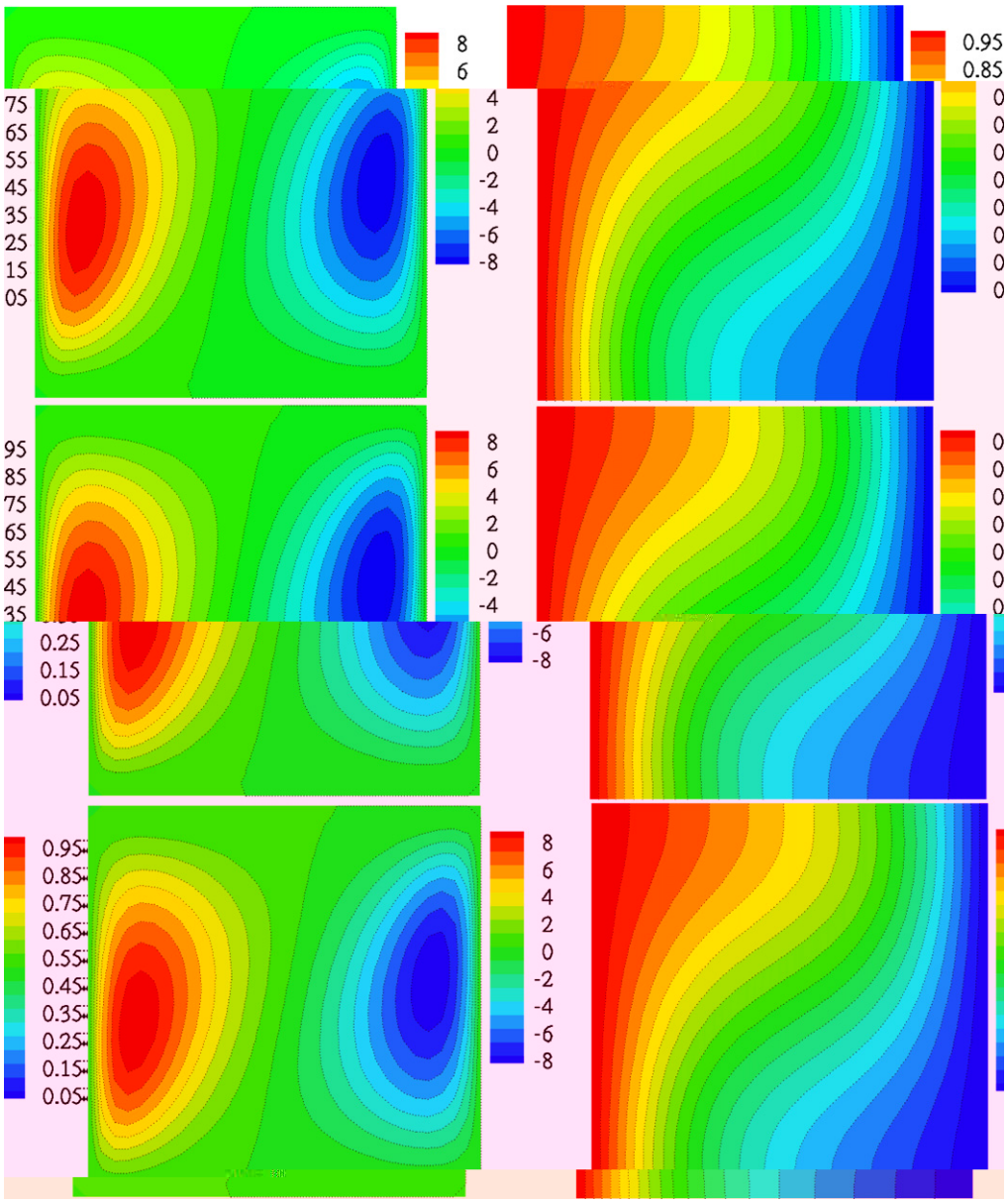

Fig. 18. Mean *v* velocity component (left) and temperature (right) contours from different solution strategies. Top row: second-order GPCE expansion; middle row: a level 5 collocation method; bottom row: Monte-Carlo sampling over 50,000 samples with 20 terms used in the K–L expansion.

5.2.6. Effect of large variation of random porosity field

In order to further demonstrate the effectiveness of the second-order stabilized stochastic projection method, we consider the same correlation function as in Eq. (51), but with a rather large variance $\sigma^2 = 9.0$. In this case, the coefficient of variation is 500%. In order to reduce the computational time, we choose the correlation length for this case as $b = 1.0$. As a result of the large variation, higher-order polynomial expansion is needed in order to capture the strong non-linear random fluctuation. Therefore, a four-dimensional third-order expansion is used in the GPCE computation, which gives a total of 35 modes. Since the correlation structure does not change from the earlier case examined, the contour pattern of each mode does not change either. Thus, we will not show these results here. The comparison of the computed standard deviation from the stochastic projection method and the Monte-Carlo sampling approach is given in Fig. 21. Note that the magnitude of standard deviation is much larger here than in the case of Fig. 19, although the contour patterns are nearly the same as expected. The large standard deviation shown results from the larger variation of the random porosity field. Thus, the present method successfully captures the highly-heterogeneous input uncertainty.

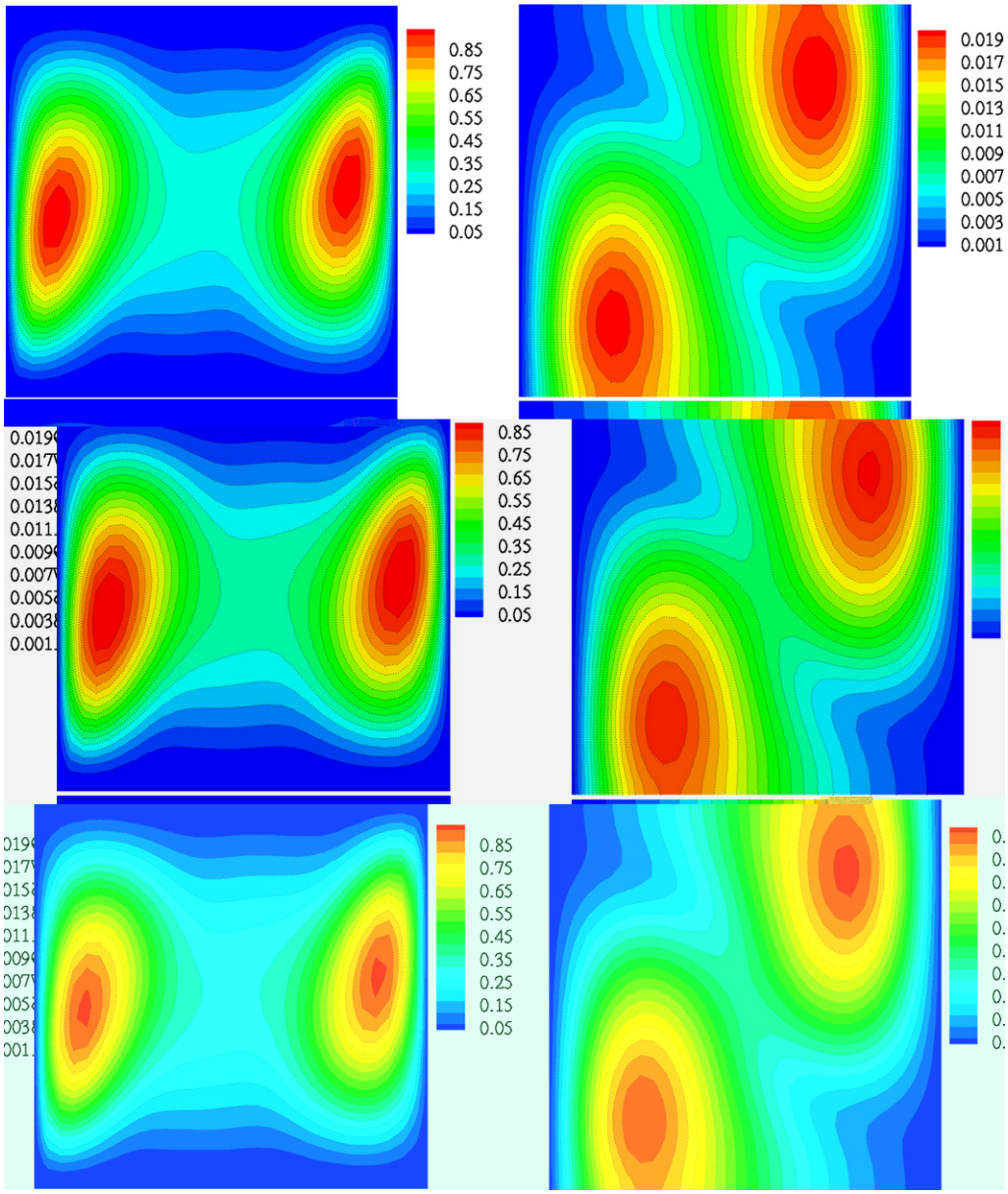

Fig. 19. Standard deviation of v velocity component (left) and temperature (right) contours from different solution strategies. Top row: second-order GPCE expansion; middle row: a level 5 collocation method; bottom row: Monte-Carlo sampling over 50,000 samples with 20 terms used in the K–L expansion.

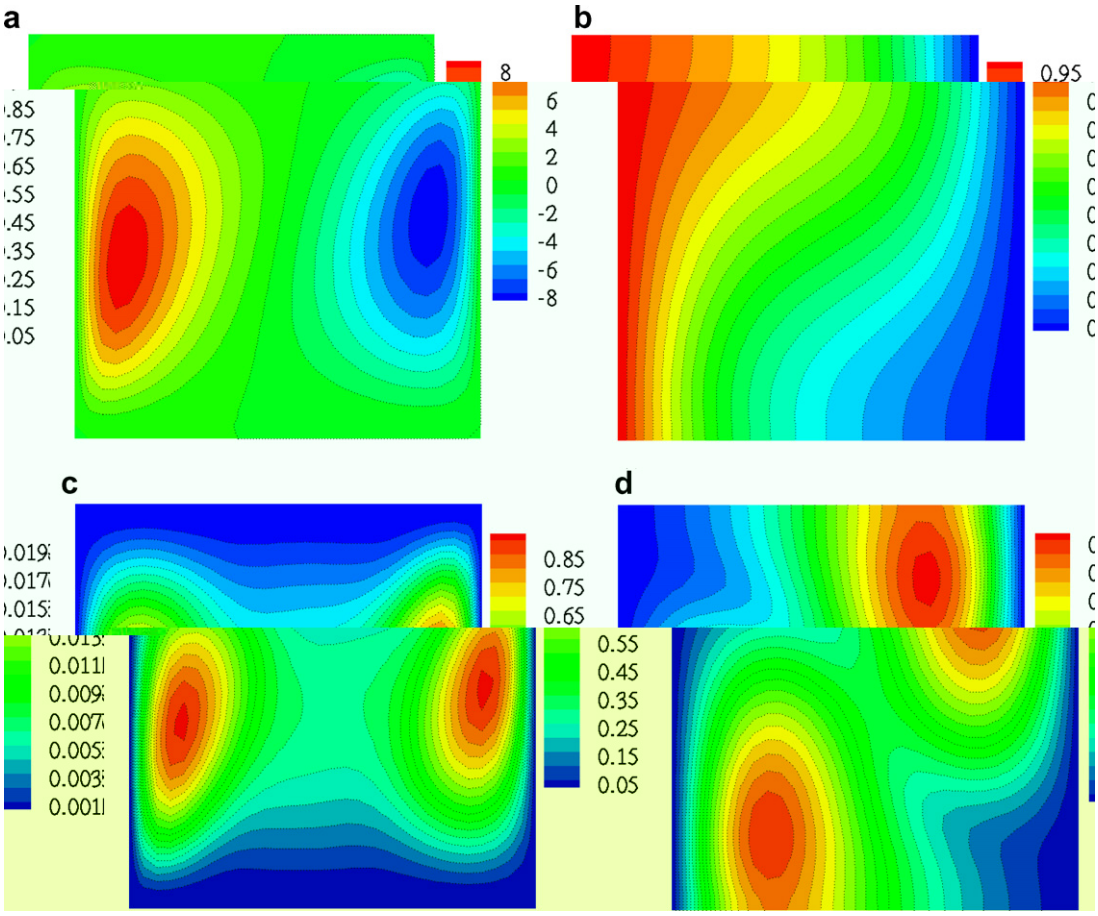

Fig. 20. Monte-Carlo sampling over 50,000 samples with 100 terms used in the K–L expansion: (a) mean v velocity component, (b) mean temperature, (c) standard deviation of v velocity component and (d) standard deviation of temperature.

6. Conclusions

A second-order stabilized stochastic projection method was used to model uncertainty propagation in natural convection in random porous media. Due to the decoupling of the calculation of velocity and pressure, the methodology can easily handle large degrees of freedom when solving the stochastic Navier–Stokes equations. In addition to a standard benchmark deterministic problem, a two-dimensional stochastic problem with moderate and large variation were examined. A detailed discussion was given to analyze the effects of the randomness on velocity and temperature. Monte-Carlo simulation and the sparse grid (Smolyak) collocation method were used to validate the present model. For the problems examined, the computation cost of the SSFEM and sparse grid simulations were similar. The MC simulations were significantly more expensive. In the SSFEM, it was shown that it is rather easy to identify dominant stochastic modes in the solution and investigate how the uncertainty propagates from porosity to the velocity and temperature random fields.

In the examples considered, the ratio of the correlation length over the domain size determines the input stochastic dimensions. For small ratios more terms in the K–L expansion are needed to capture the input uncertainty, which results in a large number of stochastic dimensions. As it is well known, the GPCE method suffers from the so called "curse of dimensionality", where the computational complexity of the problem increases combinatorially with the number of stochastic dimensions and the number of expansion terms (see Eq. (23)). Therefore, the effectiveness of the method depends on the ratio of the correlation length over the domain size. Here, we choose a rather moderate correlation length for demonstration purposes. However, it is emphasized that the method discussed here is general and not limited on the number of input stochastic dimensions provided that sufficient computational resources are available. However, in the high-dimensional case, the method is not computationally very efficient. The stochastic collocation method can serve as a very attractive alternative to the SSFEM paradigm [46]. In addition, when the stochastic dimension is moderate, the method also provides an efficient way for solving the stochastic Navier–Stokes equation which is very computational demanding if we use other stabilized methods such as in [37].

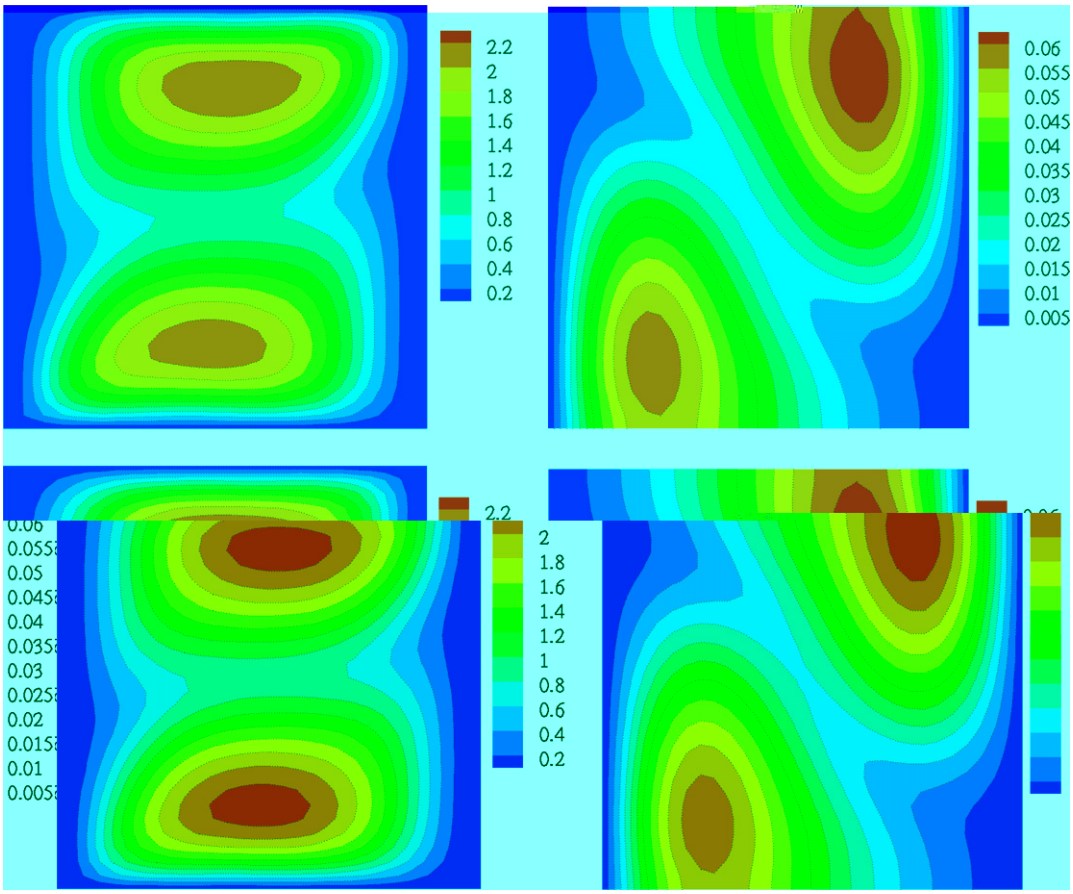

Fig. 21. Case of large variation in porosity. Comparison of the standard deviation computed with the stochastic projection method and with Monte-Carlo sampling over 50,000 samples with 100 terms used in the K–L expansion (top row: GPCE results; bottom row: Monte-Carlo results; left column: u velocity component; right column: temperature).

The key ingredient in the implementation of the algorithms presented here includes the development of a stochastic modeling library based on the GPCE formulation. This library includes computational tools for the implementation of the Askey polynomials, a parallel K–L expansion eigensolver, and a post-processing class for the calculation of higher-order solution statistics such as standard deviation and probability density function. A sparse grid collocation library based on the Smolyak algorithm has also been developed. Using such tools, one can easily convert an existing deterministic code into a code that solves the corresponding stochastic problem.

References

[1] P. Nithiarasu, K.N. Seetharamu, T. Sundararajan, Natural convective heat transfer in a fluid saturated variable porosity medium, Int. J. Heat Mass Transfer 40 (1997) 3955–3967.
[2] C.L. Winter, D.M. Tartakovsky, A. Guadagnini, Numerical solutions of moment equations for flow in heterogeneous composite aquifers, Water Resour. Res. 38 (2002) 13-1–13-8.
[3] C.L. Winter, D.M. Tartakovsky, A. Guadagnini, Moment differential equations for flow in highly heterogeneous porous media, Surv. Geophys. 24 (2003) 81–106.
[4] D.M. Tartakovsky, A. Guadagnini, M. Riva, Stochastic averaging of nonlinear flows in heterogeneous porous media, J. Fluid Mech. 492 (2003) 47–62.
[5] L.W. Gelhar, Stochastic Subsurface Hydrology, Prentice-Hall, Englewood Cliffs, NJ, 1993.
[6] G. Dagan, Flow and Transport in Porous Formations, Springer, New York, 1989.
[7] D. Zhang, Stochastic Methods for Flow in Porous Media: Coping with Uncertainties, Academic Press, San Diego, CA, 2002.
[8] R.G. Ghanem, P.D. Spanos, Stochastic Finite Elements: A Spectral Approach, Springer, New York, 1991.
[9] D. Xiu, G.E. Karniadakis, The Wiener–Askey polynomial chaos for stochastic differential equations, SIAM J. Sci. Comput. 24 (2002) 619–644.
[10] D. Xiu, G.E. Karniadakis, Modeling uncertainty in flow simulations via generalized polynomial chaos, J. Comput. Phys. 187 (2003) 137–167.
[11] O. Knio, O. Le Maître, Uncertainty propagation in CFD using polynomial chaos decomposition, Fluid Dynam. Res. 38 (2006) 616–640.
[12] D. Lucor, D. Xiu, C.-H. Su, G.E. Karniadakis, Predictability and uncertainty in CFD, Int. J. Numer. Methods Fluids 43 (2003) 483–505.
[13] B.V. Asokan, N. Zabaras, A stochastic variational multiscale method for diffusion in heterogeneous random media, J. Comput. Phys. 218 (2006) 654–676.
[14] B. Ganapathysubramanian, N. Zabaras, Modelling diffusion in random heterogeneous media: Data-driven models stochastic collocation and the variational multi-scale method, J. Comput. Phys. 226 (2007) 326–353.
[15] R. Ghanem, Probabilistic characterization of transport in heterogeneous media, Comput. Methods Appl. Mech. Engrg. 158 (1998) 199–220.

[16] R. Ghanem, Scales of fluctuation and the propagation of uncertainty in random porous media, Water Resour. Res. 34 (1998) 2123–2136.
[17] R. Ghanem, S. Dham, Stochastic finite element analysis of multiphase flow in heterogeneous porous media, Transp. Porous Media 32 (1998) 239–262.
[18] D. Xiu, G.E. Karniadakis, Modeling uncertainty in steady state diffusion problems via generalized polynomial chaos, Comput. Methods Appl. Mech. Engrg. 191 (2002) 4927–4948.
[19] D. Zhang, Z. Lu, An efficient, high-order perturbation approach for flow in random porous media via Karhunen–Loève and polynomial expansions, J. Comput. Phys. 194 (2004) 773–794.
[20] Z. Lu, D. Zhang, A comparative study on flow in uncertainty quantification for flow in randomly heterogeneous media using Monte Carlo simulations and conventional and KL-based moment-equation approaches, SIAM J. Sci. Comput. 26 (2004) 558–577.
[21] Z. Lu, D. Zhang, Stochastic simulations for flow in nonstationary randomly heterogeneous porous media using a KL-based moment-equation approach, Multiscale Model. Simul. 6 (2007) 228–245.
[22] O.P. Le Maître, O.M. Knio, H.N. Najm, R.G. Ghanem, A stochastic projection method for fluid flow: I. Basic formulation, J. Comput. Phys. 173 (2001) 481–511.
[23] O.P. Le Maître, M.T. Reagan, O.M. Knio, H.N. Najm, R.G. Ghanem, A stochastic projection method for fluid flow: II. Random process, J. Comput. Phys. 181 (2002) 9–44.
[24] O.P. Le Maître, O.M. Knio, R.G. Ghanem, H.N. Najm, A stochastic projection method for microchannel flow, Model. Simul. Microsyst. (2001) 246–249.
[25] O.P. Le Maître, M.T. Reagan, B. Debusschere, H.N. Najm, R.G. Ghanem, O.M. Knio, Natural convection in a closed cavity under stochastic non-Boussinesq conditions, SIAM J. Sci. Comput. 26 (2004) 375–394.
[26] K. Vafai, Convective flow and heat transfer in variable-porosity media, J. Fluid Mech. 147 (1984) 233–259.
[27] J.L. Guermond, P. Minev, J. Shen, An overview of projection methods for incompressible flows, Comput. Methods Appl. Mech. Engrg. 195 (2006) 6011–6045.
[28] A.J. Chorin, Numerical solution of the Navier–Stokes equations, Math. Comp. 22 (1968) 745–762.
[29] J. van Kan, A second-order accurate pressure-correction scheme for viscous incompressible flow, SIAM J. Sci. Stat. Comp. 7 (1986) 870–891.
[30] J.B. Bell, P. Colella, H.M. Glaz, A second-order projection method for the incompressible Navier–Stokes equations, J. Comput. Phys. 85 (1989) 257–283.
[31] J.L. Guermond, L. Quartapelle, On stability and convergence of projection methods based on pressure Poisson equation, Int. J. Numer. Methods Fluids 26 (1998) 1039–1051.
[32] R. Codina, J. Blasco, A finite element formulation for the Stokes problem allowing equal velocity–pressure interpolation, Comput. Methods Appl. Mech. Engrg. 143 (1997) 373–391.
[33] R. Codina, J. Blasco, Stabilized finite element method for the transient Navier–Stokes equations based on a pressure gradient projection, Comput. Methods Appl. Mech. Engrg. 182 (2000) 277–300.
[34] R. Codina, J. Blasco, G.C. Buscaglia, A. Huerta, Implementation of a stabilized finite element formulation for the incompressible Navier–Stokes equations based on a pressure gradient projection, Int. J. Numer. Methods Fluids 37 (2001) 419–444.
[35] R. Codina, Pressure stability in fractional step finite element methods for incompressible flows, J. Comput. Phys. 170 (2001) 112–140.
[36] B. Ganapathysubramanian, N. Zabaras, Sparse grid collocation schemes for stochastic natural convection problems, J. Comput. Phys. 225 (2007) 652–685.
[37] N. Zabaras, D. Samanta, A stabilized volume-averaging finite element method for flow in porous media and binary alloy solidification processes, Int. J. Numer. Methods Engrg. 60 (2004) 1–38.
[38] A. Kesse, Numerical solution of systems with stochastic uncertainties – a general purpose framework for stochastic finite elements, Ph.D. thesis, TU Braunschweig, Germany (Fachbereich Mathematik und Informatik (2004) 43–45).
[39] Scalable library for eigenvalue problem computations, <http://www.grycap.upv.es/slepc/>.
[40] Portable, extensible toolkit for scientific computation, <http://acts.nersc.gov/petsc/>.
[41] N. Wiener, The homogeneous chaos, Am. J. Math. 60 (1938) 897–936.
[42] B.J. Debusschere, H.N. Najm, P.P. Pébay, O.M. Knio, R.G. Ghanem, O.P. Le Maître, Numerical challenges in the use of polynomial chaos representations for stochastic processes, SIAM J. Sci. Comput. 26 (2004) 698–719.
[43] S. Acharjee, N. Zabaras, Uncertainty propagation in finite deformations – a spectral stochastic Lagrangian approach, Comput. Methods Appl. Mech. Engrg. 195 (2006) 2289–2312.
[44] R.L. Iman, W.J. Conover, Small sample sensitivity analysis techniques for computer models with an application to risk assessment, Commun. Statist. A 9 (1980) 1749–1842.
[45] M. Le Bars, M.G. Worster, Solidification of a binary alloy: finite-element single-domain simulation and new benchmark solutions, J. Comput. Phys. 216 (2006) 247–263.
[46] X. Ma, N. Zabaras, An adaptive hierarchical sparse grid collocation algorithm for the solution of stochastic differential equations, J. Comput. Phys., submitted for publication.